



# Dynamically Orthogonal Numerical Schemes for Efficient Stochastic Advection and Lagrangian Transport

Florian Feppon, Pierre F J Lermusiaux

## ► To cite this version:

Florian Feppon, Pierre F J Lermusiaux. Dynamically Orthogonal Numerical Schemes for Efficient Stochastic Advection and Lagrangian Transport. SIAM Review, 2018, 60 (3), pp.595 - 625. 10.1137/16m1109394 . hal-01881442

**HAL Id: hal-01881442**

**<https://hal.science/hal-01881442>**

Submitted on 25 Sep 2018

**HAL** is a multi-disciplinary open access archive for the deposit and dissemination of scientific research documents, whether they are published or not. The documents may come from teaching and research institutions in France or abroad, or from public or private research centers.

L'archive ouverte pluridisciplinaire **HAL**, est destinée au dépôt et à la diffusion de documents scientifiques de niveau recherche, publiés ou non, émanant des établissements d'enseignement et de recherche français ou étrangers, des laboratoires publics ou privés.

# DYNAMICALLY ORTHOGONAL NUMERICAL SCHEMES FOR EFFICIENT STOCHASTIC ADVECTION AND LAGRANGIAN TRANSPORT

FLORIAN FEPPON AND PIERRE F.J. LERMUSIAUX.\*

**Abstract.** Quantifying the uncertainty of Lagrangian motion can be performed by solving a large number of ordinary differential equations with random velocities, or equivalently a stochastic transport partial differential equation (PDE) for the ensemble of flow-maps. The Dynamically Orthogonal (DO) decomposition is applied as an efficient dynamical model order reduction to solve for such stochastic advection and Lagrangian transport. Its interpretation as the method that applies instantaneously the truncated SVD on the matrix discretization of the original stochastic PDE is used to obtain new numerical schemes. Fully linear, explicit central advection schemes stabilized with numerical filters are selected to ensure efficiency, accuracy, stability, and direct consistency between the original deterministic and stochastic DO advections and flow-maps. Various strategies are presented for selecting a time-stepping that accounts for the curvature of the fixed rank manifold and the error related to closely singular coefficient matrices. Efficient schemes are developed to dynamically evolve the rank of the reduced solution and to ensure the orthogonality of the basis matrix while preserving its smooth evolution over time. Finally, the new schemes are applied to quantify the uncertain Lagrangian motions of a 2D double gyre flow with random frequency and of a stochastic flow past a cylinder.

**AMS subject classifications.** 65C20, 53B21, 15A23, 35R60

**1. Introduction.** Advection plays a major role in a wide variety of physical processes and engineering applications of fluid mechanics [26, 3], neutronic transport, chemical transports, atmospheric sciences [62] and ocean sciences [20, 53]. At its most fundamental level, the pure advection process is commonly understood through the transport partial differential equation (PDE),

$$(1) \quad \begin{cases} (\partial_t + \mathbf{v}(t, \mathbf{x}) \cdot \nabla) \psi = 0 \\ \psi(0, \mathbf{x}) = \psi_0(\mathbf{x}), \end{cases}$$

that models the material transport of a passive (scalar or vectorial) tracer field  $\psi$  under a velocity field  $\mathbf{v}$ , having initially its values distributed as  $\psi_0$  over a physical domain  $\Omega \subset \mathbb{R}^d$  of positions  $\mathbf{x}$ . Another description of transport considers a parcel of material initially located at the location  $\mathbf{x}_0$  and transported to the position  $\phi_0^t(\mathbf{x}_0) = \mathbf{x}(t)$  with the instantaneous velocity  $\mathbf{v}(t, \mathbf{x}(t))$ . In this Lagrangian description,  $\mathbf{x}(t)$  is the solution of the ordinary differential equation (ODE)

$$(2) \quad \begin{cases} \dot{\mathbf{x}} = \mathbf{v}(t, \mathbf{x}(t)) \\ \mathbf{x}(0) = \mathbf{x}_0, \end{cases}$$

and  $\phi_0^t$ , *i.e.* the function mapping the initial positions  $\mathbf{x}_0$  to those  $\phi_0^t(\mathbf{x}_0) = \mathbf{x}(t)$  at time  $t$ , is the *flow-map* of the ODE (2). Under sufficient regularity conditions on the velocity field  $\mathbf{v}$  [9, 2], the solution  $\psi$  of the advection eq. (1) relates to (2) as being obtained by “carrying  $\psi_0$  values along particles’ paths”:

$$(3) \quad \psi(t, \mathbf{x}) = \psi_0((\phi_0^t)^{-1}(\mathbf{x})),$$

where  $(\phi_0^t)^{-1}$  is the backward or inverse flow-map (Figure 1).

---

\*MSEAS, Massachusetts Institute of Technology (feppon@mit.edu, pierrel@mit.edu).

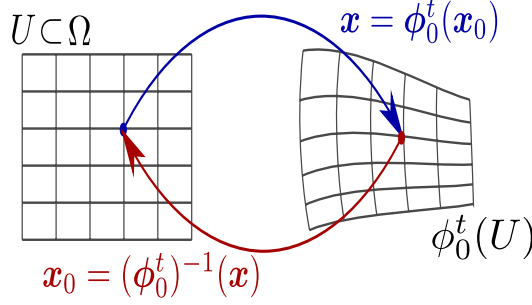


Fig. 1: Illustration of the action of the forward and backward flow-map on a subdomain  $U \subset \Omega$  of a spatial domain  $\Omega \subset \mathbb{R}^d$ .  $\phi_0^t$  maps initial particle positions  $\mathbf{x}_0$  to their position at time  $t$ , and  $(\phi_0^t)^{-1}$  is the reciprocal map.

In fact, (1) and (2) are equivalent mathematical descriptions of material transport, as setting  $\psi_0(\mathbf{x}) = \mathbf{x}$  in (3) yields  $\psi(t, \mathbf{x}) = (\phi_0^t)^{-1}(\mathbf{x})$ . Similarly, solving backward in time the transport equation with a terminal condition,

$$(4) \quad \begin{cases} (\partial_s + \mathbf{v}(s, \mathbf{x}) \cdot \nabla) \boldsymbol{\rho} = 0 \\ \boldsymbol{\rho}(t, \mathbf{x}) = \boldsymbol{\rho}^t(\mathbf{x}), \end{cases}$$

allows to retrieve the forward flow map from the relation  $\boldsymbol{\rho}(s, \mathbf{x}) = \boldsymbol{\rho}^t(\phi_s^t(\mathbf{x}))$  by setting  $\boldsymbol{\rho}^t(\mathbf{x}) = \mathbf{x}$ . This shows that the flow-map  $\phi_0^t$  can be obtained from a solution of the transport PDE (1) and vice versa. This property has been thoroughly investigated on the theoretical side to provide a mathematical meaning to the solutions of the ODE (2) for velocity fields  $\mathbf{v}$  with weak regularity [9, 2, 4], and more recently in numerical computations, as it offers an alternative method to direct particle advection for the evaluation of the flow-map  $\phi_0^t$  [44, 45].

A typical challenge encountered in environmental flow predictions is the need for dealing with velocity data that include a certain level of uncertainty, resulting from sparse data acquisitions, noise in direct measurements, or errors in the inferred numerical predictions [41]. Uncertainty is modeled by including randomness in the velocity field [39]: each realization  $\mathbf{v}(t, \mathbf{x}; \omega)$  corresponds to a particular possible scenario  $\omega$ . An issue of great interest in hazard predictions [33], is to quantify how this uncertainty reverberates in the Lagrangian motion [42]. A basic Monte-Carlo (MC) approach would then solve either the stochastic ODE

$$(5) \quad \begin{cases} \dot{\mathbf{x}} = \mathbf{v}(t, \mathbf{x}; \omega) \\ \mathbf{x}(0) = \mathbf{x}_0, \end{cases}$$

or the stochastic partial differential equation (SPDE)

$$(6) \quad \begin{cases} \partial_t \psi + \mathbf{v}(t, \mathbf{x}; \omega) \cdot \nabla \psi = 0 \\ \psi(0, \mathbf{x}) = \mathbf{x}, \end{cases}$$

for a large number of realizations,  $\omega$ . While performance of particle as well as MC methods can be optimized through parallelism, such methodologies are computationally demanding for cases requiring high resolution in both the spatial and stochastic domains, *i.e.* large numbers of particles and realizations. Hence, while they have been

useful in a variety of applications [6, 46], particle and MC methods are very expensive for uncertain advection.

A substantial benefit of the PDE formulation (6) is its compatibility with dynamical model order reduction that take direct advantage of the spatial structures in the solution. Classic reduced order methods aim to evolve low-rank decompositions such as  $\psi(t, \mathbf{x}; \omega) \simeq \sum_{i=1}^{r_\Psi} \zeta_i(t; \omega) \mathbf{u}_i(\mathbf{x})$  or  $\psi(t, \mathbf{x}; \omega) \simeq \sum_{i=1}^{r_\Psi} \zeta_i(\omega) \mathbf{u}_i(t, \mathbf{x})$  at a cost much smaller than the direct realization methods [76, 19] by independently evolving a small number  $r_\Psi$  of spatial modes,  $\mathbf{u}_i$ , or stochastic coefficients,  $\zeta_i$ . For model order reduction of stochastic PDEs, classic methods ranging from Polynomial Chaos [56, 28, 86, 13], Proper Orthogonal Decomposition (POD) [26, 60], Dynamic Mode Decomposition (DMD) [61, 67, 79, 84, 31], or stochastic Galerkin schemes and adjoint methods [10, 7] assume *a priori* choices of time-independent modes  $\mathbf{u}_i(\mathbf{x})$  and/or rely on gaussianity assumptions on the probability distribution of the coefficients  $\zeta_i$ . For example, the popular data POD [26] and DMD [67] methods suggest to extract time independent modes  $\mathbf{u}_i(\mathbf{x})$  that respectively best represent the variability (for the POD method) or the approximate linear dynamics (for the DMD method) of a series of snapshots  $\mathbf{u}(t_k, \mathbf{x}, \omega_0)$ , for a given observed or simulated realization  $\omega_0$ . These modes allow to quickly obtain information about the dynamics of this time series, and then to infer simple reduced order models for evolving the coefficients  $\zeta_i(t; \omega)$  of a more general solution  $\mathbf{u}(t, \mathbf{x}; \omega)$  by Galerkin projection. DMD and POD may be very useful and efficient methods to analyze the given time series  $\mathbf{u}(t_k, \mathbf{x}; \omega_0)$  and infer information on its *hidden* dynamics, but the use of the inferred reduced order model may be allowed only if the variability of the observed snapshot is sufficiently representative, in both time and stochastic domains, of the non-reduced stochastic solution  $\mathbf{u}(t, \mathbf{x}; \omega)$ . As it will be demonstrated hereafter, the DO equations overcome this difficulty as they allow to predict *both* the variability and the time evolution of the stochastic solution  $\mathbf{u}(t, \mathbf{x}; \omega)$  solely from its non reduced dynamics.

In general, the above methods may not be well suited for capturing low-rank solutions that do not decompose on a small number of time-invariant modes (e.g. as in POD and DMD), or that exhibit spatial irregularities not easily captured by Fourier modes (e.g. as in spectral methods), or multimodal and non-Gaussian behaviors of the coefficients (e.g. as in Polynomial Chaos methods). This is especially the case with material transport as advection tends to create fine features in the solution, with sharp gradients or shocks that evolve in time and space. Capturing them requires careful numerical schemes [55, 54, 72, 48]. Upwinding, total variation diminishing (TVD), or Essentially Non Oscillatory (ENO) schemes use diverse rules depending on the sign of the advecting velocity. How to adapt these schemes for reduced-order numerical advection, which cannot afford examining the realizations individually, is therefore particularly challenging [78, 81, 66]. This explains in part why many stochastic advection attempts have essentially restricted themselves to one dimensional applications [19, 28, 13, 56] or simplified 2D cases that do not exhibit strong shocks [82].

In contrast with these reduced order methods, the Dynamically Orthogonal (DO) methodology [63, 65] solves dynamical equations to simultaneously evolve a time-dependent basis of modes,  $\mathbf{u}_i(t, \mathbf{x})$ , and coefficients,  $\zeta_i(t; \omega)$ ,

$$(7) \quad \psi(t, \mathbf{x}; \omega) \simeq \sum_{i=1}^{r_\Psi} \zeta_i(t; \omega) \mathbf{u}_i(t, \mathbf{x}).$$

This dynamic approach [37] can efficiently capture the evolving spatial flow features and their variability at the minimal condition that such a modal approximation (7)

exists for the non-reduced solution  $\psi(t, \mathbf{x}; \omega)$  [30, 52, 17]. Numerical schemes for DO equations were derived for a variety of dynamics, from stochastic Navier-Stokes [81] to Hamilton-Jacobi [75] equations. Recently, using differential geometry, the DO equations were shown [17] to be instantaneously optimal among any other reduced order model. In fact, a non-intrusive matrix version of the DO approach was independently introduced to efficiently evolve time-dependent matrices [30]. Dynamical systems that continuously perform classic matrix operations [5, 8, 74, 12] or learn dominant Kalman filter subspaces [34, 36] have also been derived. However, critical research questions remained for stochastic DO transports. They relate to the consistency of the direct MC integration with the numerical DO integration, to the ill-conditioning of the coefficient matrix [49] (related to the curvature of the reduced-rank manifold), to the need of capturing the sharp local gradients of the advected fields, and to the issue of maintaining the numerical orthonormality of the dynamic modes.

The purpose of this article is thus to utilize the DO decomposition [63] and its geometric interpretations [17] to obtain a systematic, optimal reduced-order method for eq. (6) and to derive new numerical schemes that answer the above questions for stochastic advection and Lagrangian transports. For the latter, as an immediate benefit, a novel and efficient computational methodology for evaluating an ensemble of flow-maps  $\psi(t, \mathbf{x}; \omega) = \phi_0^t(\mathbf{x}; \omega)$  of the ODE (5) with random velocity is obtained. The issue of shock capturing is addressed by considering fully linear but stabilized advection schemes. This provides deterministic-stochastic consistency and compatible reduced-order schemes that rely on tensor decompositions of either the solution,  $\psi$ , or of its time derivative  $-\mathbf{v} \cdot \nabla \psi$ . The schemes obtained are not restricted to pure transport, they are also applicable to stochastic PDEs with advection terms of the form  $\mathbf{v} \cdot \nabla$ , such as the Navier-Stokes equations.

A synopsis of the coupled DO PDEs for the dynamical evolution of the tensor decomposition (7) is given in section 2. Numerical schemes for this set of PDEs are obtained by applying the DO methodology directly onto the spatial discretization of the stochastic transport PDE rather than its continuous version (6). In that framework, the DO equations find a rigorous geometric justification, corresponding to optimality conditions [17, 30, 52]. Section 3 focuses on the implementation in practice of the DO machinery to solve the stochastic transport PDE (6). Factorization properties of the advection operator must be preserved at the discrete level to ensure deterministic-stochastic consistency and avoid additional approximations. This is ensured through the selection of a fully linear advection scheme, whose accuracy and stability is obtained by the use of high order spatial and temporal discretization combined with linear filtering, a technique popular in ocean modeling [69, 34]. It is explained how stochastic boundary conditions can be accounted for by the model order reduced method in an optimal and convenient manner. Different possible time stepping for the DO equations are discussed, as well as the issue of modifying dynamically the stochastic dimensionality  $r_\Psi$  of the tensor approximation (7). Finally, as a requirement of both the DO method and multi-steps time marching schemes, an efficient method is proposed for preserving the orthonormality of the modal basis ( $\mathbf{u}_i$ ) during the time integration, as well as the smooth evolution of this basis and the coefficients  $\zeta_i$ . Numerical results of the overall methodology are presented in section 4 using the bi-dimensional stochastic analytic double-gyre flow and stochastic flow past a cylinder, both of which include sharp gradients. The DO results are finally contrasted with those of direct Monte-Carlo.

**Notations.** Important notations are summarized below:

$\Omega \subset \mathbb{R}^d$	Spatial domain
$\mathbf{x} \in \Omega$	Spatial position
$\mathbf{v}(t, \mathbf{x}; \omega)$	Stochastic velocity field
$\psi(t, \mathbf{x}; \omega) \simeq \sum_{k=1}^{r_\Psi} \zeta_k(t; \omega) \mathbf{u}_k(t, \mathbf{x})$	Rank $r_\Psi$ tensor approximation of the stochastic solution of the transport PDE (6)
$\mathcal{M}_{l,m}$	Space of $l$ -by- $m$ real matrices
$\Psi_{i,\alpha}(t) \simeq \psi(t, \mathbf{x}_i; \omega_\alpha)$	Full rank discrete approximation $\Psi(t) \in \mathcal{M}_{l,m}$ of the continuous solution $\psi$
$U_{i,k}(t) = \mathbf{u}_k(t, \mathbf{x}_i), Z_{\alpha,k}(t) = \zeta_k(t; \omega_\alpha)$	Discrete approximation of the modes and the coefficients with $U \in \mathcal{M}_{l,r_\Psi}, U^T U = I, Z \in \mathcal{M}_{m,r_\Psi}$ and $\text{rank}(Z) = r_\Psi$
$\mathcal{M} = \{\Psi \in \mathcal{M}_{l,m}   \text{rank}(\Psi) = r_\Psi\}$	Fixed rank matrix manifold
$\Psi(t) = U(t)Z(t)^T \in \mathcal{M}$	Rank $r_\Psi$ approximation of the discretized solution $\Psi(t)$
$\mathcal{T}(\Psi)$	Tangent space at $\Psi \in \mathcal{M}$
$\mathcal{N}(\Psi)$	Normal space at $\Psi \in \mathcal{M}$
$\Pi_{\mathcal{T}(\Psi)}$	Orthogonal projection onto the plane $\mathcal{T}(\Psi)$
$\Pi_{\mathcal{M}}$	Orthogonal projection onto $\mathcal{M}$ or rank $r_\Psi$ -truncated SVD
$I$	Identity mapping
$A^T$	Transpose of a square matrix $A$
$\langle A, B \rangle = \text{Tr}(A^T B)$	Frobenius scalar product for matrices
$\langle \mathbf{u}, \mathbf{v} \rangle$	$L^2$ scalar product for functions $\mathbf{u}, \mathbf{v}$ over $\Omega \subset \mathbb{R}^d$
$\ A\  = \text{Tr}(A^T A)^{1/2}$	Frobenius norm
$\sigma_1(A) \geq \dots \geq \sigma_{\text{rank}(A)}(A)$	Non zeros singular values of $A \in \mathcal{M}_{l,m}$
$\dot{\Psi} = d\Psi/dt$	Time derivative of a rank $r_\Psi$ solution $\Psi$
$\rho_\Psi$	Retraction on the manifold $\mathcal{M}$ at $\Psi \in \mathcal{M}$

## 2. Dynamically Orthogonal stochastic transport equations.

**2.1. Mathematical setting for the transport PDE.** The stochastic transport PDE (6) is set on a smooth bounded domain  $\Omega$  of  $\mathbb{R}^d$  where  $d$  denotes the spatial dimension. The flow-map  $\phi_0^t$  of the ODE (5) is defined for all time if particle trajectories don't leave the domain  $\Omega$ , which is ensured if the normal flux  $\mathbf{v} \cdot \mathbf{n}$  vanishes on the boundary  $\partial\Omega$ ,  $\mathbf{n}$  denoting the outward normal of  $\Omega$ . In the following, one deals with the more general case where  $\mathbf{v} \cdot \mathbf{n}$  may have an arbitrary sign on  $\partial\Omega$ . Inlet and outlet boundaries are denoted respectively

$$\begin{aligned} \partial\Omega_-(t; \omega) &= \{x \in \partial\Omega | \mathbf{v}(t, x; \omega) \cdot \mathbf{n} < 0\} \\ \partial\Omega_+(t; \omega) &= \{x \in \partial\Omega | \mathbf{v}(t, x; \omega) \cdot \mathbf{n} \geq 0\}, \end{aligned}$$

Boyer [4] has shown that the transport eq. (6) is well posed (under suitable regularity assumptions on  $\mathbf{v}$ ), provided a Dirichlet boundary condition is prescribed at the inlet  $\partial\Omega_-(t; \omega)$ . Following Leung [44], this work considers the Dirichlet boundary condition

$$(8) \quad \psi(t, \mathbf{x}; \omega) = \mathbf{x} \text{ on } \partial\Omega_-(t; \omega),$$

which ensures that the solution  $\psi(t, \mathbf{x}; \omega)$  carries the value of the initial entering location of the particle that arrived in  $\mathbf{x}$  at time  $t$ . Theoretically, no boundary condition is required on the outlet boundary  $\partial\Omega_+(t; \omega)$ , but some conditions may be used for convenience, e.g. for numerical schemes that do not use upwinding rules. In the applications of section 4, the Neumann boundary condition was considered:

$$(9) \quad \frac{\partial \psi}{\partial \mathbf{n}}(t, \mathbf{x}; \omega) = 0 \text{ on } \partial\Omega_+(t; \omega),$$

which is a boundary condition previously implemented in [44], and which naturally arises when considering  $\psi$  as a viscous limits of eq. (6) (see Theorem 4.1 in [4]). Such zero normal flux condition can be interpreted as due to artificial viscosity that instantaneously diffuses trajectories normally to the outlet. For simplicity, it is assumed

that a dynamic modal decomposition of the stochastic velocity field  $\mathbf{v}$  is available:

$$(10) \quad \mathbf{v}(t, \mathbf{x}; \omega) = \sum_{k=1}^{r_v} \beta_k(t; \omega) \mathbf{v}_k(t, \mathbf{x}),$$

which can be obtained by truncating the Karhunen-Loeve expansion [58].

**2.2. The DO field equations.** The DO field equations evolve adaptive modes  $\mathbf{u}_i(t, \mathbf{x})$  and stochastic coefficients  $\zeta_i(t; \omega)$  considered both as time-dependent quantities, so as to most accurately update the modal approximation (7). Such equations can formally be found by replacing the solution  $\boldsymbol{\psi}$  with its tensor approximation (7) in the transport eq. (6) :

$$(11) \quad (\partial_t \zeta_j) \mathbf{u}_j + \zeta_j \partial_t \mathbf{u}_j + \zeta_j \beta_k \mathbf{v}_k \cdot \nabla \mathbf{u}_j = 0,$$

where the Einstein summation convention over repeated indexes is used. The family of modes is assumed orthonormal, namely

$$(12) \quad \forall 1 \leq i, j \leq r_\Psi, \quad \langle \mathbf{u}_i, \mathbf{u}_j \rangle = \int_{\Omega} (\mathbf{u}_i(t, \mathbf{x}), \mathbf{u}_j(t, \mathbf{x})) d\mathbf{x} = \delta_{ij},$$

where  $\langle, \rangle$  and  $(,)$  denote the scalar products respectively on  $L^2(\Omega)$  and on the space  $\mathbb{R}^d$ . Furthermore, without loss of generality, the “dynamically orthogonal condition”

$$(13) \quad \forall 1 \leq i, j \leq r_\Psi, \quad \langle \partial_t \mathbf{u}_i, \mathbf{u}_j \rangle = 0$$

is imposed to remove the redundancy in (7), coming from the fact that the modal decomposition is invariant under rotations of modes  $\mathbf{u}_i$  and coefficients  $\zeta_i$  [64, 17]. Equations for the coefficients,  $\zeta_i$ , are then obtained by  $L^2$  projection of (11) onto the modes,  $\mathbf{u}_i$ :

$$(14) \quad \forall 1 \leq i \leq r_\Psi, \quad \partial_t \zeta_i + \zeta_j \beta_k \langle \mathbf{v}_k \cdot \nabla \mathbf{u}_j, \mathbf{u}_i \rangle = 0.$$

Governing equations for the modes,  $\mathbf{u}_i$ , are obtained by  $L^2$  projection on the space of the stochastic coefficients: multiplying (11) by  $\zeta_i$ , replacing  $\partial_t \zeta_j$  using (14) yields:

$$\zeta_i (-\zeta_l \beta_k \langle \mathbf{v}_k \cdot \nabla \mathbf{u}_l, \mathbf{u}_j \rangle) \mathbf{u}_j + \zeta_i \zeta_j \partial_t \mathbf{u}_j + \zeta_i \zeta_j \beta_k \mathbf{v}_k \cdot \nabla \mathbf{u}_j = 0,$$

which allows obtaining, after taking the expectation and multiplying by the inverse  $(\mathbb{E}[\zeta_i \zeta_j])^{-1}$  of the symmetric moment matrix  $(\mathbb{E}[\zeta_i \zeta_j])_{1 \leq i, j \leq r_\Psi}$ :

$$(15) \quad \partial_t \mathbf{u}_i + (\mathbb{E}[\zeta_i \zeta_j])^{-1} \mathbb{E}[\zeta_i \zeta_j \beta_k] \mathbf{v}_k \cdot \nabla \mathbf{u}_j = (\mathbb{E}[\zeta_i \zeta_j])^{-1} \mathbb{E}[\zeta_i \zeta_l \beta_k] \langle \mathbf{v}_k \cdot \nabla \mathbf{u}_l, \mathbf{u}_j \rangle \mathbf{u}_j.$$

Deriving boundary conditions is slightly more delicate as (8) and (9) involve a stochastic partition  $\partial\Omega = \partial\Omega_-(t; \omega) \cup \partial\Omega_+(t; \omega)$  of the boundary. They are obtained again by inserting (7) into the original eqs. (8) and (9), which can then be rewritten

$$\sum_{j=1}^{r_\Psi} \left[ \zeta_j \mathbf{u}_j \mathbf{1}_{\mathbf{v} \cdot \mathbf{n} < 0} + \zeta_j \frac{\partial \mathbf{u}_j}{\partial \mathbf{n}} \mathbf{1}_{\mathbf{v} \cdot \mathbf{n} \geq 0} \right] = \mathbf{x} \mathbf{1}_{\mathbf{v} \cdot \mathbf{n} < 0} \text{ on } \partial\Omega,$$

where  $\mathbf{1}_{\mathbf{v} \cdot \mathbf{n} < 0}(t, \mathbf{x}; \omega)$  is the random indicator variable equal to 1 when  $\mathbf{v} \cdot \mathbf{n} < 0$  and 0 otherwise, and  $\mathbf{1}_{\mathbf{v} \cdot \mathbf{n} \geq 0} = 1 - \mathbf{1}_{\mathbf{v} \cdot \mathbf{n} < 0}$ . Projecting again on the space of coefficients,  $\zeta_i$ , yields mixed boundary conditions for the modes,  $\mathbf{u}_i$  :

$$(16) \quad \mathbb{E}[\zeta_i \zeta_j \mathbf{1}_{\beta_k \mathbf{v}_k \cdot \mathbf{n} < 0}] \mathbf{u}_j + \mathbb{E}[\zeta_i \zeta_j \mathbf{1}_{\beta_k \mathbf{v}_k \cdot \mathbf{n} \geq 0}] \frac{\partial \mathbf{u}_j}{\partial \mathbf{n}} = \mathbb{E}[\zeta_i \mathbf{1}_{\beta_k \mathbf{v}_k \cdot \mathbf{n} < 0}] \mathbf{x} \text{ on } \partial\Omega.$$

The reader is referred to [21] for further developments on DO boundary conditions.

So far, the coupled PDEs for DO modes and coefficients (14)–(16) have been derived *first* [64, 75, 52] and numerical schemes developed thereafter [81]. In doing so, the numerical consistency between the original SPDE (6) and the model order reduced system (14)–(16) should be respected. In addition, since unadapted discretizations of the convective terms  $\mathbf{v} \cdot \nabla \psi$  in eq. (1) can lead to instability (blowing up) of the numerical solution, a great deal of attention must be given to the discretization of the modal fluxes  $\mathbf{v}_k \cdot \nabla \mathbf{u}_j$ . Popular advection schemes [47, 54] utilize up-winding, in the sense that spatial derivatives are discretized according to the orientation of the full velocity,  $\mathbf{v}$ . When the velocity  $\mathbf{v}$  becomes stochastic, this is not an issue for direct MC solutions of (6), but for reduced order equations such as (14)–(16), special care is needed to ensure stability without having recourse to expensive MC evaluations. These difficulties were acknowledged in previous works dealing with stochastic Navier-Stokes equations. For example, an empirical remedy consists of averaging numerical fluxes according to the probability distribution of the velocity direction [81]. In the following, it is shown that these issues can in fact be more directly addressed by using the geometric matrix framework investigated in [17].

### 2.3. Geometric framework in matrix spaces and theoretical guarantees.

Instead of seeking numerical schemes for the continuous DO equations (14)–(16), it is numerically useful to apply the DO methodology directly on the spatial discretization chosen for the original SPDE (6). The results then indicate consistent discretizations of DO equations, assuming these are well-posed, i.e. DO discretizations that still accurately simulate each discretized deterministic realizations.

At the spatially discrete level, realizations of the solution vector field are represented in computer memory by the entries of a  $l$ -by- $m$  matrix  $\Psi_{i,j}(t) = \psi(t, \mathbf{x}_i; \omega_j)$ , where  $l$  denotes the total spatial dimension (typically  $l/d$  nodes  $\mathbf{x}_i$  are used for a  $d$ -dimensional domain) and  $m$  realizations  $\omega_j$  are considered. The numerical solution  $\Psi(t)$  of the SPDE (6) is obtained by solving the matrix ODE

$$(17) \quad \dot{\Psi} = \mathcal{L}(t, \Psi),$$

where  $\mathcal{L}$  is a matrix operator that includes spatial discretizations of the realizations of the fluxes  $-\mathbf{v} \cdot \nabla \psi$ , and of the boundary conditions (8). In that context, model order reduction consists in approximating the solution of the large  $l$ -by- $m$  ODE system (17) by a low rank decomposition

$$(18) \quad \Psi(t) \simeq \Psi(t) = U(t)Z(t)^T$$

similarly as in (7), where  $U(t)$  and  $Z(t)$  are respectively lower dimensional  $l$ -by- $r_\Psi$  and  $m$ -by- $r_\Psi$  matrices containing the discretizations  $U_{ik}(t) = \mathbf{u}_k(t, \mathbf{x}_i)$  and  $Z_{jk}(t) = \zeta_k(t; \omega_j)$  of the modes and coefficients. The orthonormality of modes (12) and the DO condition (13) then require that the columns of  $U$  are orthonormal and orthogonal to their derivatives, namely

$$(19) \quad U^T U = I \text{ and } U^T \dot{U} = 0,$$

where  $I$  is the  $r_\Psi$ -by- $r_\Psi$  identity matrix. In this matrix framework, the DO methodology can be rigorously formulated as a dynamical system on the manifold

$$\mathcal{M} = \{\Psi \in \mathcal{M}_{l,m} | \text{rank}(\Psi) = r_\Psi\}$$



of rank  $r_\Psi$  matrices embedded in the space  $\mathcal{M}_{l,m}$  of  $l$ -by- $m$  matrices. In all what follows, the bold notation  $\Psi \in \mathcal{M}_{l,m}$  is used to refer to matrices of the ambient space  $\mathcal{M}_{l,m}$  whose rank,  $\text{rank}(\Psi)$ , is in general greater than  $r_\Psi$ . The non-bold notation  $\Psi \in \mathcal{M}$  refers to rank  $r_\Psi$  matrices on the manifold. The DO approximation  $\Psi(t)$  is defined to be the dynamical system on  $\mathcal{M}$  geometrically obtained by replacing the vector field  $\mathcal{L}(t, \cdot)$  with its tangent projection [17, 30]:

$$(20) \quad \begin{cases} \dot{\Psi} &= \Pi_{\mathcal{T}(\Psi)}(\mathcal{L}(t, \Psi)) \\ \Psi(0) &= \Pi_{\mathcal{M}}(\Psi(0)), \end{cases}$$

where the notation  $\Pi_{\mathcal{M}}$  denotes the orthogonal projection onto the manifold  $\mathcal{M}$  and  $\Pi_{\mathcal{T}(\Psi)}$  the orthogonal projection onto its tangent space at the point  $\Psi$  (see Figure 2).

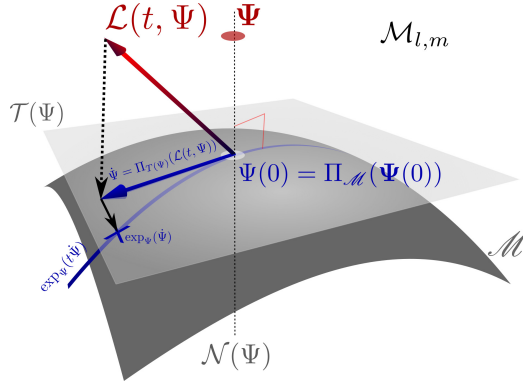


Fig. 2: Geometric interpretation of the DO approximation and of the exponential map  $\exp_R$ . The time derivative  $\mathcal{L}(t, R)$  is replaced by its best tangent approximation. Schematic adapted from [83].

Given the choices (18) and (19), the ODE system (20) can be written as a set of coupled evolution equations for the mode and coefficient matrices  $U$  and  $Z$ , that turn to be exactly a discrete version of the continuous DO equations (14) and (15):

$$(21) \quad \begin{cases} \dot{Z} = \mathcal{L}(t, UZ^T)^T U \\ \dot{U} = (I - UU^T)\mathcal{L}(t, UZ^T)Z(Z^T Z)^{-1}. \end{cases}$$

The orthogonal projection  $\Pi_{\mathcal{M}}$  onto  $\mathcal{M}$  used for the initialization of  $\Psi(0)$  is nothing else than the application that maps the matrix  $\Psi$  onto its best rank  $r_\Psi$  approximation, *i.e.* the truncated Singular Value Decomposition (SVD) [27] (such approach was used to initialize ocean uncertainty predictions [40, 38]). The SVD of the original numerical solution is the discrete analogous of the Karhunen-Loeve decomposition:

$$\Psi = \sum_{i=1}^{\text{rank}(\Psi)} \sigma_i(\Psi) u_i v_i^T,$$

where  $\sigma_1(\Psi) \geq \dots \geq \sigma_{\text{rank}(\Psi)}(\Psi) > 0$  are the singular values of  $\Psi$  and  $u_i$  and  $v_i$  orthonormal families of left and right singular vectors. The truncated SVD is the algebraic operation that removes modes of order higher than  $r_\Psi$ :

$$(22) \quad \Pi_{\mathcal{M}}(\Psi) = \sum_{i=1}^{r_\Psi} \sigma_i(\Psi) u_i v_i^T \in \mathcal{M}.$$

Feppon et Lermusiaux [17] have shown that the dynamical system (20) applies instantaneously the truncated SVD to constrain the rank of the reduced solution  $\Psi$  at all times. In other words, it is the continuous limit when  $\Delta t \rightarrow 0$  of the solution that would be obtained by systematically applying the truncated SVD after any Euler (or any other explicit time discretization) time step:

$$(23) \quad \Pi_{\mathcal{T}(\Psi)}(\mathcal{L}(t, \Psi)) = \lim_{\Delta t \rightarrow 0} \frac{\Pi_{\mathcal{M}}(\Psi + \Delta t \mathcal{L}(t, \Psi)) - \Psi}{\Delta t}.$$

Therefore (20) yields an optimal time-evolution of the modal decomposition  $\Psi = UZ^T$  at least for small integration times. More theoretical guarantees have been obtained in [17], where it is proven that the error of the DO approximation (20) is controlled by the best truncation error  $\|\Psi(t) - \Pi_{\mathcal{M}}(\Psi(t))\|$  as long as the original solution  $\Psi(t)$  remains at a close distance to the set  $\mathcal{M}$  of low rank matrices, which translates into the algebraic condition

$$\sigma_{r_\Psi}(\Psi(t)) > \sigma_{r_\Psi+1}(\Psi(t)),$$

i.e. singular values of order  $r_\Psi$  and  $r_\Psi + 1$  do not cross (a condition previously observed numerically in [30, 52]).

### 3. Implementation of the DO approximation for stochastic advection.

Exploiting the geometric framework, new schemes for the DO approximation (21) of the stochastic transport equation (6) are obtained. High-order linear stabilized advection schemes that maintain sharp spatial gradients and deterministic-stochastic consistency are presented (subsection 3.1). Stochastic DO boundary conditions derived from optimality criteria are discussed (subsection 3.2). Time-marching strategies for the DO equations, using the truncated SVD and the retractions [1] for maintaining the numerical solution on the low-rank manifold, are obtained and contrasted: direct Euler, exponential map from geodesic equations, and algebraic and gradient-descent-based time-marching (subsection 3.3). Finally, accurate methods for dynamically evolving the rank of the DO subspace and for preserving the orthonormality of the modes and their smooth evolution are derived (subsections 3.4 and 3.5).

**3.1. Motivations for linear advection schemes.** The DO approximation is computationally attractive because (21) evolves a solution constrained to the low-rank manifold of – small – dimension  $(l+m)r_\Psi - r_\Psi^2$  (by evolving the  $lr_\Psi + mr_\Psi$  coefficients of the matrices  $U$  and  $Z$  with  $U$  orthonormal), instead of the initial  $lm$  independent matrix coefficients of the original high dimensional dynamical system (17). As a consequence, the DO matrix system (21) offers a true gain of computational efficiency *only* if the evaluation of  $l$ -by- $m$  matrices can be avoided. This is not a priori achievable in a direct non-intrusive scheme if the operator  $\mathcal{L}$  needs to be evaluated on the  $l$ -by- $m$  matrix  $\Psi = UZ^T$ . If all  $lm$  coefficients of  $\Psi$  were needed to be computed from  $U$  and  $Z$ , there would be no computational benefit other than a reduction of memory storage in comparison with solving the original non-reduced system (17). The gain of efficiency can be achieved if the operator  $\mathcal{L}(t, \cdot)$  maps a rank  $r_\Psi$  decomposition  $\Psi = UZ^T$  onto a factorization

$$(24) \quad \mathcal{L}(t, UZ^T) = L_U L_Z^T$$

of rank at most  $r_L$ , where  $L_U$  is a  $l$ -by- $r_L$  matrix,  $L_Z$  a  $m$ -by- $r_L$  matrix, and  $r_L$  an integer typically largely inferior to  $l$  and  $m$ . In that case, the system (21) can be computed efficiently as

$$(25) \quad \begin{cases} \dot{Z} = L_Z [L_U^T U] \\ \dot{U} = [(I - UU^T)L_U][L_Z^T Z(Z^T Z)^{-1}]. \end{cases}$$

where brackets have been used to highlight products that allow computing the derivatives  $\dot{U}$  and  $\dot{Z}$  without having to deal with  $l$ -by- $m$  matrices. Such factorization occurs for instance when  $\mathcal{L}(t, \cdot)$  is polynomial of order  $d$ , for which rank  $r_\Psi$  matrices are mapped onto rank  $r_L \leq (r_\Psi)^d$  matrices.

In the spatially continuous view point, the differential operator  $\psi \mapsto \mathbf{v} \cdot \nabla \psi$  satisfies this condition, as the rank  $r_\Psi$  decomposition (7) is mapped to one of rank  $r_L = r_\Psi \times r_v$ :

$$(26) \quad \mathbf{v} \cdot \nabla \psi = \sum_{\substack{1 \leq j \leq r_\Psi \\ 1 \leq k \leq r_v}} \zeta_j \beta_k \mathbf{v}_k \cdot \nabla \mathbf{u}_j.$$

This equation further highlights why adapting advection schemes to model order reduction is challenging, as popular discretizations of  $\mathbf{v} \cdot \nabla \psi$  involve non-polynomial nonlinearities in the matrix operator  $\mathcal{L}$ . These schemes rely indeed on the use of min-max functions required by upwinding or high order discretizations such as ENO or TVD schemes that select a smooth approximation of the spatial derivative  $\nabla \psi$ , e.g. [78]. In these cases, the nonlinearity of the operator  $\mathcal{L}$  prevents the decomposition (26) to hold at the discrete level without introducing further approximations, which may alter drastically the stability of time integration and the accuracy of the numerical solution. A very natural approach followed by [64, 81] is to assume that the decomposition (26) holds before applying nonlinear schemes to discretize the fluxes  $\mathbf{v}_k \cdot \nabla \mathbf{u}_j$  in (14) and (15). A key issue then is to maintain consistency between the deterministic MC and stochastic DO solutions. Indeed, in the examples considered in section 4 for which high gradients occur, such approaches were at times observed to lead to either numerical explosion or significant errors for long integration times.

Consequently, this work investigated the use of linear central advection schemes that do not require upwinding and that have the property to preserve the decomposition (26). Therefore, the advection  $-\mathbf{v} \cdot \nabla \psi$  is discretized as

$$(27) \quad \mathcal{L}(t, \Psi)_{i,\alpha} = -\mathbf{v}(t, \mathbf{x}_i; \omega_\alpha) \cdot \mathbf{D} \Psi_{i,\alpha}$$

where  $\mathbf{D}$  is a linear finite-difference operator approximating the gradient  $\nabla$ . With  $\Psi = UZ^T$  as in (18), this yields the decomposition  $\mathcal{L}(t, \Psi) = L_U L_Z^T$  as required in (25), where  $L_U$  and  $L_Z$  are the  $l$ -by- $r_L$  and  $m$ -by- $r_L$  matrices

$$(L_U)_{i,jk} = \mathbf{v}_k(t, \mathbf{x}_i) \cdot \mathbf{D} \mathbf{u}_j(t, \mathbf{x}_i), \quad (L_Z)_{\alpha,jk} = \zeta_j(t; \omega_\alpha) \beta_k(t, \omega_\alpha).$$

In one dimension, the gradient can be approximated by the second order operator

$$(28) \quad \mathbf{D} \Psi_{i,\alpha} = \frac{\Psi_{i+1,\alpha} - \Psi_{i-1,\alpha}}{2\Delta x},$$

and this article will also consider the sixth order finite difference operator

$$(29) \quad \mathbf{D} \Psi_{i,\alpha} = \frac{3}{2} \frac{\Psi_{i+1,\alpha} - \Psi_{i-1,\alpha}}{2\Delta x} - \frac{3}{5} \frac{\Psi_{i+2,\alpha} - \Psi_{i-2,\alpha}}{4\Delta x} + \frac{1}{10} \frac{\Psi_{i+3,\alpha} - \Psi_{i-3,\alpha}}{6\Delta x},$$

where  $\Delta x$  denotes the spatial resolution and a natural numbering is assumed for the index  $i$ . These formula are adapted in a straightforward manner to discretize partial derivatives in higher dimension [54]. This approach might seem unexpected, since central schemes are known to be numerically unstable under Euler time integration. In addition, the Godunov theorem expresses that it is not possible to devise a linear

scheme higher than first order accuracy that do not create false extrema in numerical solutions [18]. These extrema are produced by numerical dispersion and manifest under the form of spurious oscillations. In fact, it is possible to contain this phenomenon near shocks, and obtain high order accuracy where the solution is smooth. Stability and the removal of part of the oscillations can be achieved by the introduction of a right amount of numerical dissipation, either using artificial viscosity [73] or filtering [69, 14, 32, 59, 11]. Shapiro filters are especially attractive because they are easy to implement, fully linear, and designed to remove optimally the shortest resolvable numerical frequency without affecting other wave components [69, 70, 71]. In one dimension, denoting  $\delta^2$  the operator  $\delta^2 \Psi_{i,\alpha} = \Psi_{i+1,\alpha} - 2\Psi_{i,\alpha} + \Psi_{i-1,\alpha}$ , the Shapiro filters  $\mathcal{F}^{(i)}$  of order  $i = 2, 4$  and  $8$  are defined by the formulas (see [69])

$$(30) \quad \begin{aligned} \mathcal{F}^{(2)} \Psi_{i,\alpha} &= (1 + \delta^2/4) \Psi_{i,\alpha} \\ \mathcal{F}^{(4)} \Psi_{i,\alpha} &= (1 - \delta^2/4)(1 + \delta^2/4) \Psi_{i,\alpha} \\ \mathcal{F}^{(8)} \Psi_{i,\alpha} &= (1 + \delta^4/16)(1 - \delta^4/16) \Psi_{i,\alpha}. \end{aligned}$$

The order and frequency of applications can be tuned to the desired filter-spectrum [34]. Their linearity allows to filter the decomposition  $\psi = \zeta_i \mathbf{u}_i$  efficiently by filtering the discretization of the modes  $\mathbf{u}_i$ , or in other words,  $\mathcal{F}^{(i)}(U Z^T) = (\mathcal{F}^{(i)} U) Z^T$ . Critically, this DO filtering is consistent with the filtering of MC realizations.

To achieve further stability, higher order discretizations of the temporal derivative are generally used in complement to these filters. Popular linear multi-step methods range from Leap-Frog [85], Runge-Kutta and Adam Bashforth [11]. For instance, for a time increment  $\Delta t$ , the second order Leap-Frog scheme evolves the value  $\Psi^n$  of the numerical solution  $\Psi$  at time  $t^n = n\Delta t$  according to the rule

$$(31) \quad \frac{\Psi^{n+1} - \Psi^{n-1}}{2\Delta t} = \mathcal{L}(t^n, \Psi^n),$$

while the third order Runge Kutta (RK3) method uses

$$(32) \quad \frac{\Psi^{n+1} - \Psi^n}{\Delta t} = \frac{k_1^n + 4k_2^n + k_3^n}{6} \text{ with } \begin{cases} k_1^n &= \mathcal{L}(t^n, \Psi^n) \\ k_2^n &= \mathcal{L}(t^n + \Delta t/2, \Psi^n + k_1^n \Delta t/2) \\ k_3^n &= \mathcal{L}(t^n + \Delta t, \Psi^n + \Delta t(2k_2^n - k_1^n)). \end{cases}$$

A comparison of several combinations of these techniques is illustrated in Figure 3 for the one dimensional advection equation  $\partial_t \psi + v \partial_x \psi = 0$ , a benchmark case for selecting an appropriate linear scheme for the transport eq. (6) in higher dimension. A boxcar function is advected to the right with a velocity  $v = 0.7$  in the domain  $[0, 1]$  until the time  $t = 10$ . The spatial resolution is set to  $\Delta x = 0.002$  and the CFL condition  $\Delta t \leq 0.6v\Delta x$  is used to define the time increment  $\Delta t$ . The figure illustrates how accuracy and stability can be achieved by (i) using multi-step time marching schemes, (ii) using high order spatial discretization and (iii) adding a proper amount of numerical dissipation to remove spurious oscillations. We note that linear limiters may also be combined with Shapiro filters [24], maintaining consistency.

**3.2. Boundary conditions.** Boundary conditions (BCs) of the reduced solution have been formally obtained in section 2. They could be treated more rigorously by incorporating original BCs (8) and (9) directly within the discretization of the operator  $\mathcal{L}$ . However, this approach can lead to a more complex implementation. In this work, boundary nodes are stored in a  $l_{bc} \times m$  “ghost” matrix and it is assumed that the  $l$ -by- $m$  matrix of realizations  $\Psi$  contains only the values at internal nodes.

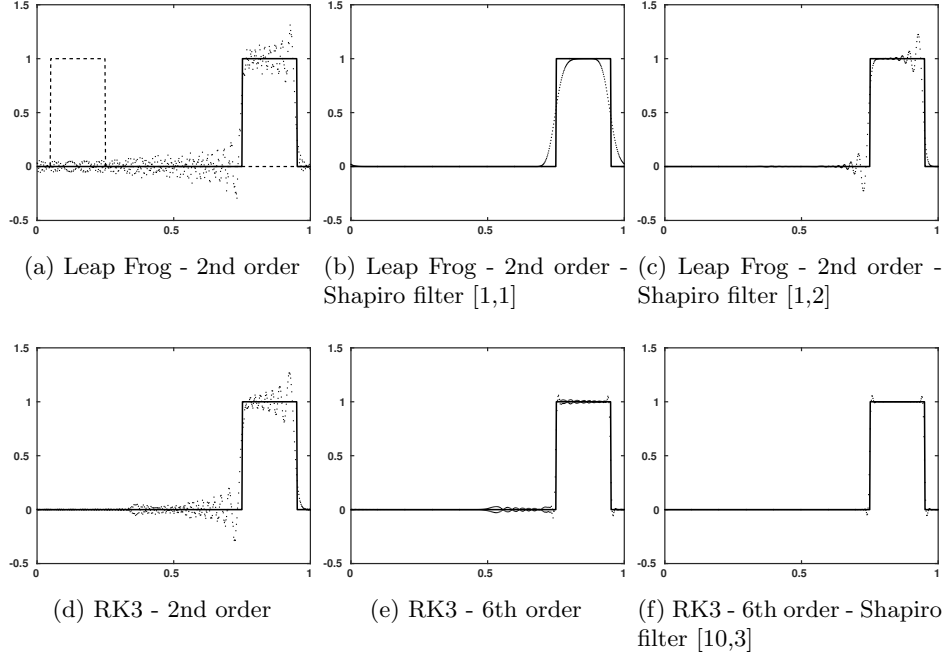


Fig. 3: Comparison of the numerical solution (*dotted line*) with the analytical solution (*solid line*) of the 1D advection equation for different linear centered schemes. The text “Shapiro filter  $[n_1, n_2]$ ” indicates that the Shapiro filter of order  $2^{n_2}$  (see [69]) has been applied after every  $n_1$  iterations. The initial box-car function is visible in dashed line on the first plot.

These ghost cells allow convenient evaluation of the differential operator  $D$  in the definition (27) of  $\mathcal{L}(t, \Psi)$ . Their values are reinitialized at the beginning of each time step according to the BCs (8) and (9). In the following, the operator which assigns the values of these boundary cells at time  $t$  is denoted  $\mathcal{B}_C(t, \cdot)$ , i.e. the discrete BCs are then explicit (if implicit, they are solved for simultaneously with the interior solution, e.g. see [21]). With this notation, the solution that includes both internal nodes and boundary values is the block matrix  $\Psi_{bc} = \begin{bmatrix} \mathcal{B}_C(t, \Psi) \\ \Psi \end{bmatrix}$ . For example, on the one-dimensional domain  $\Omega = [0, 1]$ , the value of the boundary node  $\mathbf{x}_1 = 0$  is determined by the relation

$$\mathcal{B}_C(t, \Psi)_{1,\alpha} = \begin{cases} 0 & \text{if } v(t, 0; \alpha) \geq 0 \\ (18\Psi_{2,\alpha} - 9\Psi_{3,\alpha} + 2\Psi_{4,\alpha})/11 & \text{if } v(t, 0; \alpha) < 0, \end{cases}$$

if one uses a third order reconstruction for the Neumann BC (9). The difficulty of determining how these BCs should be accounted for by the reduced solution  $\Psi = UZ^T$  comes from the fact that assigning boundary values does in general not preserve the rank: i.e.  $\text{rank}(\Psi_{bc}) > r_\Psi$  (in practice, the rank of this interior+boundary DO solution should be large enough to represent both the reduced interior solution and reduced BCs, see [21]). BCs may be enforced on the reduced solution while ensuring minimal

error by solving the minimization problem

$$(33) \quad \min_{\text{rank}(\Psi_{bc})=r_\Psi} \left\| \Psi_{bc} - \begin{bmatrix} \mathcal{B}_C(t, \Psi) \\ \Psi \end{bmatrix} \right\|^2.$$

This yields the best rank  $r_\Psi$  approximation of the  $(l + l_{bc})$ -by- $m$  matrix  $\Psi_{bc}$ , whose decomposition  $\Psi_{bc} = U_{bc}Z_{bc}^T$  allows to compute conveniently the discrete differential operator  $D$  in (27) requiring boundary values. The minimization can for example be achieved by using a gradient descent starting from the initial rank  $r_\Psi$  matrix  $\Psi$ , as explained in the next subsection and in [17, 50].

When BCs are deterministic or homogeneous, they can be directly implemented as BCs for the discretization of the modes,  $\mathbf{u}_i$  [63]. For example, zero Dirichlet or Neumann BCs for all the realizations of  $\psi$  directly corresponds to the same BCs for the modes,  $\mathbf{u}_i$ . For more general cases, it is usually desirable to avoid solving (33) and to instead obtain BCs for the modes that optimally approximate the original BCs. This is achieved by replacing the minimization problem (33) with that for the  $l_{bc}$ -by- $r_\Psi$  ghost matrix  $U_{bc}$  containing boundary values for the matrix  $U$ :

$$(34) \quad \min_{U_{bc} \in \mathcal{M}_{l_{bc}, r_\Psi}} \|U_{bc}Z^T - \mathcal{B}_C(t, \Psi)\|^2.$$

The solution of this linear regression problem is easily obtained by writing the stationarity condition

$$\forall \delta U \in \mathcal{M}_{l_{bc}, r_\Psi}, \quad 2 \langle \delta U \rangle Z^T, U_{bc}Z^T - \mathcal{B}_C(t, \Psi) \rangle = 0,$$

which eventually yields

$$(35) \quad U_{bc} = \mathcal{B}_C(t, \Psi)Z(Z^TZ)^{-1}.$$

It turns out that this optimality condition is the discrete analogous of the original BCs (16) obtained formally in section 2. The decomposition of the reduced solution including boundary values considered is therefore  $\Psi_{bc} = \begin{bmatrix} U_{bc} \\ U \end{bmatrix} Z^T$ . Further discussions on DO BCs are provided in [21].

**3.3. Low-rank time-stepping.** One issue commonly encountered in the time discretization of dynamical systems is the fact that the discrete time stepping tends to make the numerical solution exit the manifold  $\mathcal{M}$  where the trajectories live. If  $\Psi^n$  is a point on the manifold  $\mathcal{M}$  at  $t^n$ , and  $\dot{\Psi}^n \in \mathcal{T}(R)$  is the time derivative, any straight move  $\Psi^n + \Delta t \dot{\Psi}^n$  leaves the fixed rank manifold  $\mathcal{M}$ . An application, called *retraction*, must be used to convert the tangent direction  $X = \Delta t \dot{\Psi}^n \in \mathcal{T}(\Psi^n)$  into a point  $\rho_{\Psi^n}(X)$  back onto the manifold. A retraction  $\rho_{\Psi^n} : \mathcal{T}(\Psi^n) \rightarrow \mathcal{M}$  (Figure 2) is an application describing how to move on the manifold in a tangent direction  $X \in \mathcal{T}(\Psi^n)$  starting from  $\Psi^n \in \mathcal{M}$ . By definition, it must satisfies the consistency conditions that (i) a zero velocity results in a null move, *i.e.*  $\rho_{\Psi^n}(0) = \Psi^n$ , and (ii) a move in the  $X$  direction results in a trajectory on  $\mathcal{M}$  with  $X$  as initial speed :  $\frac{d}{dt} \rho_{\Psi^n}(tX)|_{t=0} = X$  (see [1]). The ideal retraction is the *exponential map* that follows geodesics or shortest paths on the manifold, but may be expensive to evaluate. In practice, one uses approximations of this map that leads to several strategies of implementations for the explicit discretization of (21).

### 3.3.1. Direct time marching scheme for the matrix DO system (21).

As in [81, 52], a very intuitive idea for moving a rank  $r_\Psi$  matrix  $\Psi^n = U^n Z^{nT}$  onto a direction  $\dot{\Psi}^n = \dot{U}^n Z^{nT} + U^n \dot{Z}^{nT}$  with a step  $\Delta t$  is to update independently the mode and coefficient matrices  $U^n$  and  $Z^n$  by using the following scheme, which is a direct Euler time-discretization of the system (21):

$$(36) \quad \begin{cases} Z^{n+1} = Z^n + \Delta t \dot{Z}^n \\ U^{n+1} = U^n + \Delta t \dot{U}^n, \end{cases}$$

where  $\dot{Z}^n$  and  $\dot{U}^n$  are the approximations of the time derivatives  $\dot{U}$  and  $\dot{Z}$  being used. This corresponds to using the retraction  $\rho_{UZ^T}$  defined by

$$(37) \quad \rho_{UZ^T}(\dot{U}Z^T + U\dot{Z}^T) = (U + \dot{U})(Z + \dot{Z})^T = UZ^T + (\dot{U}Z^T + U\dot{Z}^T) + \dot{U}\dot{Z}^T.$$

### 3.3.2. The exponential map : geodesic equations in between time steps.

The ideal retraction is the exponential map  $\rho_{\Psi^n} = \exp_{\Psi^n}$  (see [1]) computed from geodesic paths  $\gamma(s)$  on  $\mathcal{M}$ , which are the direct analogous of straight lines onto curved manifolds. These curves, parametrized as  $\gamma(s) = \exp_{\Psi^n}(s\dot{\Psi}^n)$  (see Figure 2), indicate the shortest way to “walk” onto the manifold from  $\Psi^n$  into the straight direction  $\dot{\Psi}^n = \dot{U}^n(Z^n)^T + U^n(\dot{Z}^n)^T$ . The value of  $\exp_{\Psi^n}(s\dot{\Psi}^n)$  is given by the solution  $\gamma(s) = U(s)Z(s)^T$  at time  $s$  of the geodesic equations [17]

$$(38) \quad \begin{cases} \ddot{Z} - Z\dot{U}^T\dot{U} &= 0. \\ \ddot{U} + U\dot{U}^T\dot{U} + 2\dot{U}\dot{Z}^T Z(Z^T Z)^{-1} &= 0 \\ U(0) = U^n, Z(0) &= Z^n \\ \dot{U}(0) = \dot{U}^n, \dot{Z}(0) &= \dot{Z}^n. \end{cases}$$

Without direct analytical solutions to (38), numerical schemes are used. Computing retractions that approximate well the exponential map is a challenge commonly encountered in optimization on matrix manifolds with orthogonality constraints [50], as discussed in [1]. One can show that the retraction  $\rho_{UZ^T}$  of equation (37) is approximating the exponential map only to the first order (see [1]), which can lead to numerical errors at locations of high curvature on the manifold  $\mathcal{M}$ . The curvature of the rank  $r_\Psi$  manifold  $\mathcal{M}$  at the point  $\Psi^n$  is inversely proportional to the lowest singular value  $\sigma_{r_\Psi}(\Psi^n)$  [17]. As a consequence, errors can be incurred by the direct time stepping (36) when the matrix  $Z^n$  is ill conditioned. Equations (38) can be solved during the DO time integration in between time steps, to move more accurately on the manifold without the need for recomputing values of the operator  $\mathcal{L}$ . For instance, Euler steps (36) can be replaced with

$$(39) \quad U^{n+1}(Z^{n+1})^T = \exp_{\Psi^n}(\Delta t \dot{\Psi}^n).$$

This can be done using high order time marching schemes for the discretization of (38). The intermediate time step  $\delta t < \Delta t$  for these can be set adaptively: a rule of thumb is to use steps in the ambient space having a length lower than the minimal curvature radius  $\sigma_{r_\Psi}(Z)$  at the point  $UZ^T$ :

$$\delta t \|\dot{U}Z^T + U\dot{Z}^T\| < C\sigma_{r_\Psi}(Z),$$

where  $C \simeq 1$  is a constant set by the user. Note that a lower order retraction such as (37) is commonly used anyway in the time discretization of the geodesic equations (38).

### 3.3.3. Direct computation of the truncated SVD at the next time step.

As highlighted in [section 2](#), DO eqs. (25) define a dynamical system that truncates the SVD at all instants so as to optimally constrain the rank of the reduced solution (23). Denoting  $\Psi^n = U^n(Z^n)^T$  the DO solution at time  $t^n$ , integrating the non-reduced dynamical system (17) for a time step  $[t^n, t^{n+1}]$  yields a rank  $r_{\mathcal{L}} > r_{\Psi}$  prediction

$$(40) \quad \Psi^{n+1} = \Psi^n + \Delta t \overline{\mathcal{L}(t^n, \Psi^n)},$$

where  $\overline{\mathcal{L}(t^n, \Psi^n)}$  represent the full-space integral for the exact integration or the increment function for a numerical integration. For the latter, it can be an approximation of the time derivative  $\mathcal{L}(t^n, \Psi(t^n))$ , e.g.  $\overline{\mathcal{L}(t^n, \Psi^n)} = \mathcal{L}(t^n, \Psi^n)$  for explicit Euler.

One way to proceed for evolving the low rank approximation  $\Psi^n$  to  $\Psi^{n+1}$  is to compute directly the rank  $r_{\Psi}$  SVD truncation  $\Pi_{\mathcal{M}}(\Psi^{n+1})$  (eq. (22))

$$(41) \quad \Psi^{n+1} = U^{n+1}(Z^{n+1})^T = \Pi_{\mathcal{M}}(\Psi^n + \Delta t \overline{\mathcal{L}(t^n, \Psi^n)})$$

so as to obtain modes and coefficients  $U^{n+1}$  and  $Z^{n+1}$  at time  $t^{n+1} = t^n + \Delta t$ . Such scheme has been shown to be a consistent time-discretization of the DO equations (20) (see [17]). For an Euler step, it corresponds to using the retraction  $\rho_{\Psi}(X) = \Pi_{\mathcal{M}}(\Psi + X)$ , a second-order accurate approximation of the exponential map [1] and hence an improvement of the direct Euler time marching (36).

*a. Computing algebraically the truncated SVD.* The scheme (41) can be computed efficiently and in a fully algebraic manner when the operator  $\mathcal{L}$  factors as (24). Indeed, the linear approximation of the time derivative then admits a decomposition  $\overline{\mathcal{L}(t^n, U^n(Z^n)^T)} = L_U^n (L_Z^n)^T$  of rank at most  $r_{\mathcal{L}} = r_L \times p_t$ ,  $p_t$  being the order of the time integration scheme utilized. Therefore  $\Psi^{n+1}$  factors as

$$(42) \quad \begin{aligned} \Psi^{n+1} &= U^n (Z^n)^T + \Delta t L_U^n (L_Z^n)^T \\ &= \Psi_U^{n+1} (\Psi_Z^{n+1})^T \text{ with } \Psi_U^{n+1} = [U^n \ L_U^n] \text{ and } \Psi_Z^{n+1} = [Z^n \ \Delta t L_Z^n], \end{aligned}$$

with  $L_U^n \in \mathcal{M}_{l, r_{\mathcal{L}}}$ ,  $L_Z^n \in \mathcal{M}_{m, r_{\mathcal{L}}}$ . The rank of  $\Psi^{n+1}$  is therefore at most  $\text{rank}(\Psi^{n+1}) = r_{\Psi} < r_{\Psi} + r_{\mathcal{L}}$  which can be assumed to be largely inferior to  $l$  and  $m$ . This can be exploited to compute the truncated SVD through an algorithm that avoids computing large matrices of size  $l$ -by- $m$  (see [Algorithm 1a](#)).

This first algorithm has some issues. First, reorthonormalizations and eigenvalue decompositions such as in steps 1 and 2 do not allow to keep track of the smooth evolution of the modes  $U(t)$  and coefficients  $Z(t)$  solutions of the system (21). Additional procedures are needed [81, 80]. Second, with the repeated use of such algebraic operations, additional round off errors may be introduced.

*b. Using gradient descent for continuous updates of the truncated SVD.* Alternatively, a gradient descent on the low-rank manifold  $\mathcal{M}$  can be used to find the correction that needs to be added to modes  $U^n$  and coefficients  $Z^n$ , so as to evaluate the SVD truncation  $\Psi^{n+1} = \Pi_{\mathcal{M}}(\Psi^{n+1})$  (eqs. (41) and (42)). Indeed,  $\Psi^{n+1} = U^{n+1}(Z^{n+1})^T$  (eq. (41)) is the minimizer of

$$J(UZ^T) = \frac{1}{2} \|\Psi_U^{n+1} (\Psi_Z^{n+1})^T - UZ^T\|^2,$$

where  $\|\cdot\|$  is the Frobenius norm. The (covariant) gradient  $\nabla J$  used for this minimization must be aligned with the maximum ascent direction tangent to  $\mathcal{M}$  at  $UZ^T$ . Its value can be shown to be  $\nabla J = (\nabla J_U)Z^T + U(\nabla J_Z)^T$  (see [17]), where  $\nabla J_U$



---

**Algorithm 1a** Rank  $r_\Psi$  truncated SVD of  $\Psi = \Psi_U \Psi_Z^T$  with  $\Psi_U \in \mathcal{M}_{l, r_\Psi}$ ,  $\Psi_Z \in \mathcal{M}_{m, r_\Psi}$  and  $r_\Psi < r_\Psi = \text{rank}(\Psi) \ll \min(l, m)$

---

- 1: Orthonormalize the columns of the matrix  $\Psi_U$  (see the discussion in [subsection 3.5](#)), *i.e.* find a basis change matrix  $A \in \mathcal{M}_{r_\Psi, r_\Psi}$  such that  $(\Psi_U A)^T (\Psi_U A) = I$  and set

$$\Psi_U \leftarrow \Psi_U A, \Psi_Z \leftarrow \Psi_Z A^{-T}$$

so as to preserve the product  $\Psi = \Psi_U \Psi_Z^T$ .

- 2: Compute the “compact” SVD of the *smaller*  $m$ -by- $r_\Psi$  matrix  $\Psi_Z$ :

$$\Psi_Z = V \Sigma P^T,$$

where  $\Sigma$  is a  $r_\Psi$ -by- $r_\Psi$  diagonal matrix of singular are values, and  $V \in \mathcal{M}_{m, r_\Psi}$  and  $P \in \mathcal{M}_{r_\Psi, r_\Psi}$  orthogonal matrices of singular vectors. This is achieved by computing the eigen decomposition of the “covariance” matrix  $\Psi_Z^T \Psi_Z$ .

- 3: The SVD of  $\Psi = \Psi_U \Psi_Z^T$  is given by  $\Psi = U \Sigma V^T$  with  $U = \Psi_U P$  an orthogonal  $l$ -by- $r_\Psi$  matrix of left singular vectors. The truncated SVD of order  $r_\Psi$  is straightforwardly obtained from the first  $r_\Psi$  columns of  $U, V$  and  $\Sigma$ .
- 

and  $\nabla J_Z$  provide respective ascent directions for the individual matrices  $U$  and  $Z$ . Their expression and the resulting gradient descent towards the updated truncated SVD  $U^{n+1}(Z^{n+1})^T$  starting from the approximate initial guess  $\Psi^n = U^n(Z^n)^T$  are detailed in [Algorithm 1b](#). Note that [\[17\]](#) proved that the procedure is convergent for almost every initial data. If in addition,  $\Delta t$  is small enough, the method is expected

---

**Algorithm 1b** Gradient descent for updating a rank  $r_\Psi$  truncated SVD of  $\Psi = \Psi_U \Psi_Z^T$  with  $\Psi_U \in \mathcal{M}_{l, r_\Psi}$ ,  $\Psi_Z \in \mathcal{M}_{m, r_\Psi}$  and  $r_\Psi < r_\Psi = \text{rank}(\Psi) \ll \min(l, m)$

---

- 1: Initialize a rank  $r_\Psi$  guess  $U_0 Z_0^T \simeq \Psi$  with  $U_0 \in \mathcal{M}_{l, r_\Psi}$ ,  $Z_0 \in \mathcal{M}_{m, r_\Psi}$ ,  $U_0^T U_0 = I$ .
- 2: To minimize  $J(U, Z) = J(U Z^T) = \|\Psi - U Z^T\|$  on  $\mathcal{M}$ , compute the gradient step

$$(43) \quad \begin{cases} Z_{k+1} = Z_k - \mu \nabla J_U(U_k, Z_k) \\ U_{k+1} = U_k - \mu \nabla J_Z(U_k, Z_k), \end{cases}$$

where  $\mu$  is a small enough constant set by the user and the gradients  $(\nabla J_U, \nabla J_Z)$  are given by (see Proposition 36 in [\[17\]](#))

$$(44) \quad \begin{cases} \nabla J_Z(U, Z) = Z - \Psi_Z [(\Psi_U)^T U] \\ \nabla J_U(U, Z) = -(I - U U^T) \Psi_U [(\Psi_Z)^T Z (Z^T Z)^{-1}], \end{cases}$$

where brackets highlight matrix products that render the computation efficient.

- 3: Orthonormalize the modes  $U_{k+1}$  (see [subsection 3.5](#)) after each iteration and repeat step 2.–3. until convergence is achieved.
- 

to converge after only a small number of iterations, while preserving the continuous evolution of the mode and coefficient matrix  $U$  and  $Z$ . In comparison with the use of geodesics, this method ensures the accuracy of the reduced solution, while being less sensitive to the singularity of the matrix  $Z$ . Also, it is a direct extension of the DO time stepping [\(36\)](#), as one step of [\(36\)](#) coincides with the first step of the gradient descent [\(43\)](#) starting from the current value  $U^n(Z^n)^T$  and with  $\mu = 1$  [\[17\]](#).

**3.4. Increasing dynamically the rank of the approximation.** In the SPDE (6), all realizations of the solution share the same initial value  $\psi(0, \mathbf{x}; \omega) = \mathbf{x}$ . Hence the DO approximation coincides with the exact solution at time  $t = 0$  and is given by the rank 1 decomposition  $\Psi = UZ^T$  where  $U$  is a normalized column vector proportional to the discretization of the coordinate function  $\mathbf{x}$ , and  $Z$  a column vector identically equal to the normalization factor. Obviously,  $\psi(t, \mathbf{x}; \omega)$  becomes random after  $t > 0$  and hence the rank of the DO solution must be increased immediately [65, 81] and modified dynamically to capture dominant stochastic subspaces that are forming throughout the time evolution of the solution. This is a common issue in model order reduction of stochastic PDEs.

Reducing the dimension  $r_\Psi$  of the DO stochastic subspace is straightforward: it is sufficient to truncate the SVD of the current DO solution  $\Psi = UZ^T$ , using for example Algorithm 1a, when the lowest singular value  $\sigma_{r_\Psi}(\Psi) < \underline{\sigma}$  becomes lower than a threshold  $\underline{\sigma}$  [65]. Increasing the stochastic dimension from  $r_\Psi$  to  $r_{\Psi'} > r_\Psi$  is more involved, as  $r_{\Psi'} - r_\Psi$  new dominant directions  $\mathbf{u}_i$  supporting the decomposition (7) must be found. The overall topic is linked to breeding schemes [29], directions of maximum error growth e.g. [57] and non-normal modes [16, 15, 51], but our emphasis here is on accurately capturing the present and evolving dominant uncertainties in the SVD sense, as in [43, 35, 65]. One approach [65] consists of assuming that uncertainties are small and uniform in the orthogonal complement of the present DO subspace and then add modes aligned with the most sensitive directions of the operator  $\mathcal{L}$  in this complement, if their growth is fast enough. This computation is based on the gradient of  $\mathcal{L}$  in the ambient space  $\mathcal{M}_{l,m}$ , and MC perturbations, but it does not guarantee tracking the best rank  $r_{\Psi'}$  approximation at the next time step. An additional difficulty lies in the issue of detecting when the dimension of the DO subspace should be increased. Sapsis and Lermusiaux [65] suggested to increase the rank  $r_\Psi$  when  $\sigma_{r_\Psi}(\Psi) > \bar{\sigma}$  reaches another threshold  $\bar{\sigma} > \underline{\sigma}$ .

These issues can be solved by examining the component of the time derivative  $\mathcal{L}(t, \Psi)$  that is normal to the manifold, i.e.  $N(UZ^T) = (I - \Pi_{\mathcal{T}(UZ^T)})(\mathcal{L}(t, UZ^T)) \in \mathcal{N}(\Psi)$ , and neglected by the DO approximation (see Figure 2). The value of this component is given by (see Prop. 35 in [17])

$$(45) \quad N(UZ^T) = (I - UU^T)\mathcal{L}(t, UZ^T)(I - Z(Z^T Z)^{-1}Z^T).$$

Since the singular value  $\sigma_{r_\Psi+1}(\Psi^n + \Delta t \overline{L(t^n, \Psi^n)})$  after a step  $\Delta t$  is of magnitude  $\sigma_1(N(\Psi^n))\Delta t$  (see [27]), this first and other singular values of  $N(UZ^T)$  are related to the speed at which the solution exits the rank  $r_\Psi$  matrix manifold  $\mathcal{M}$ . Thus, a quantitative criterion that can track the rank of the true original solution is

$$(46) \quad \sigma_1(N(U^n(Z^n)^T))\Delta t > \bar{\sigma}.$$

A common value  $\sigma$  can be used for the threshold  $\sigma = \bar{\sigma} = \underline{\sigma}$  to detect when the rank of the DO subspace must be decreased/increased, hence the setting of this single  $\sigma$  provides a lower bound desired for the smallest singular value of the covariance matrix  $Z$ . Singular vectors of  $N(U^n(Z^n)^T)$  contain the new dominant directions. They can be combined with a gradient descent similar to (43), so as to compute the rank  $r_{\Psi'}$  (instead of  $r_\Psi$ ) truncated SVD of  $\Psi^{n+1} = \Psi^n + \Delta t \overline{L(t^n, \Psi^n)}$ , while preserving the smooth evolution of the first  $r_\Psi$  modes and coefficients (in contrast with the direct use of the algebraic Algorithm 1a). The procedure is summarized in Algorithm 2.

**3.5. Preserving the orthonormality of the mode matrix  $U$ .** As highlighted in [81], an issue with time discretization, e.g. (36) or (43), is that in general, the  $l$ -

**Algorithm 2** Augmenting the rank of the DO solution

- 
- 1: Compute  $\Psi^{n+1} = U^n(Z^n)^T + \Delta L_U^n (L_Z^n)^T$  with  $L_U^n \in \mathcal{M}_{l,r_L}$ ,  $L_Z^n \in \mathcal{M}_{m,r_L}$  as in (42).
  - 2: Compute the normal component (of rank at most  $r_L$ ) at  $t^n$ .

$$N(U^n(Z^n)^T) = [(I - U^n(U^n)^T)L_U^n][(L_Z^n)^T(I - Z^n((Z^n)^T Z^n)^{-1}(Z^n)^T)].$$

- 3: Compute the rank  $r_\Psi' - r_\Psi < r_L$  truncated SVD of  $N(U^n(Z^n)^T)$ , i.e.  $N_U^n(N_Z^n)^T$ , using Algorithm 1a.
  - 4: Use the gradient descent (43) starting from the initialization values  $U_0 = [U^n N_U^n]$  and  $Z_0 = [Z^n N_Z^n]$ , so as to find the truncated SVD of rank  $r_\Psi' > r_\Psi$  of  $\Psi^{n+1}$ , i.e.  $U^{n+1}(Z^{n+1})^T$ .
- 

by- $r_\Psi$  matrix  $U^{n+1} \in \mathcal{M}_{l,r_\Psi}$  obtained after a discrete time step does not exactly satisfy the orthogonality constraint  $U^{n+1T}U^{n+1} = I$ . A numerical procedure must therefore be used to reduce the truncation errors committed by the discretization, even though the true trajectory  $U(t)Z^T(t)$  on  $\mathcal{M}$  and the DO equations (21) ensure and assume  $U^T U = I$  at all instants. This procedure must be accurate as numerical orthonormalization may also introduce round off errors that can lead to significant error over large integration times. For example, standard and modified Gram Schmidt orthonormalization present numerical instabilities when  $UZ^T$  becomes close to being rank deficient (see [77]). For this reason, [80, 81] used the following procedure: compute the eigendecomposition of the Gram matrix  $K = U^T U$ ,

$$(47) \quad PKP^T = \Sigma.$$

Then rotate and scale accordingly modes and coefficients by setting

$$(48) \quad \begin{cases} U \leftarrow UP\Sigma^{-1/2} \\ Z \leftarrow ZP\Sigma^{1/2}. \end{cases}$$

The eigenvalue problem (47) can be solved using Householder factorization which is known to be numerically stable in comparison with Gram Schmidt orthonormalization [77]. An issue is that this procedure may introduce permutations or sign changes, leading to artificial discontinuities in the time evolution of the mode and coefficient matrices  $U$  and  $Z$ . Figure 4 illustrates the problem by plotting the typical evolution of a coefficient of the matrix  $Z$  with this orthonormalization procedure. Even though sign checks alleviate the problem [81], they are a burden. Hence, to reinforce orthogonality between time steps and provide smooth evolutions for both  $U$  and  $Z$  (21), one can employ a gradient flow, as was done in the DO time-stepping (43). Reorthonormalization is then performed by finding an invertible matrix  $A \in \mathcal{M}_{r_\Psi, r_\Psi}$  such that  $(UA)^T(UA) = A^T K A = I$  and by setting  $U \leftarrow UA$  and  $Z \leftarrow ZA^{-T}$ . Such matrix  $A$  is actually the minimizer over  $\mathcal{M}_{r_\Psi, r_\Psi}$  of the functional

$$G(A) = \frac{1}{4} \|A^T K A - I\|^2.$$

Therefore, one can find a reorthonormalization matrix  $A$  close to the identity by solving the gradient flow

$$(49) \quad \frac{dA}{ds} = -\frac{dG}{dA} = -KA(A^T K A - I),$$

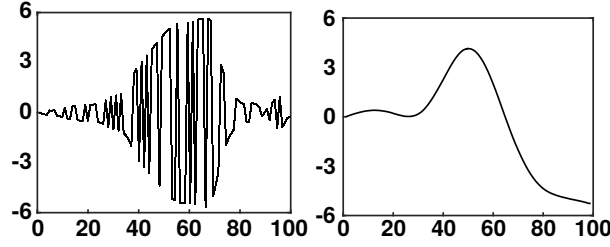


Fig. 4: Evolution of a coefficient of the matrix  $Z^n$  obtained by the time integration of (21) as a function of the iteration number. On the *left*, reorthonormalization of the matrix  $U^n$  is performed by solving the eigenvalue problem (48), while on the *right*, the gradient flow (49) was used. Eigenvalue decompositions introduce sign flips and permutations, that results in artificial discontinuities in the individual matrices  $U^n$  and  $Z^n$  if dealt algebraically [81].

with the initial value  $A(0) = I$ . The inverse  $A^{-1}$  of  $A$  can be simultaneously tracked by solving the ODE

$$\frac{dA^{-1}}{ds} = -A^{-1} \frac{dA}{ds} A^{-1}.$$

The resulting numerical procedure is summarized in Algorithm 3. Typically, one expects  $A = I + O(\|U^T U - I\|)$  and hence both corrections  $UA \simeq U$  and  $ZA^{-T} \simeq Z$  will have an order of magnitude identical to the initial error, hence ensuring the smooth evolution of  $U$  and  $Z$ . Figure 4 shows the time evolution of a coefficient of the matrix  $Z$  using this method. Only a few number of Euler steps are necessary to obtain convergence, which makes the method efficient. The matrix  $A \simeq I$  is well conditioned and the Algorithm 3 has small round off errors.

---

**Algorithm 3** Reorthonormalization procedure of  $UZ^T \in \mathcal{M}$  with  $U^T U \simeq I$

---

- 1: Define a tolerance parameter  $\epsilon$  and a time step  $\mu$  (typically  $\mu \simeq 1$ )
  - 2:  $K \leftarrow U^T U$
  - 3:  $A \leftarrow I, A^{-1} \leftarrow I$
  - 4: **while**  $\|A_k^T K A_k - I\|^2 > \epsilon$  **do**
  - 5:    $dA_k \leftarrow -K A_k (A_k^T K A_k - I)$
  - 6:    $A_{k+1} \leftarrow A_k + \mu dA_k$
  - 7:    $A_{k+1}^{-1} \leftarrow A_k^{-1} - \mu A_k^{-1} (dA_k) A_k^{-1}$
  - 8:    $k \leftarrow k + 1$
  - 9: **end while**
  - 10:  $U \leftarrow U A_k$  and  $Z \leftarrow Z A_k^{-T}$
- 

## 4. Numerical results.

**4.1. Stochastic double gyre flow.** The double gyre is the classic 2D benchmark flow for the study of Lagrangian coherence of particle motions [68, 44, 25]. The idealized flow consists of two vortices oscillating horizontally. Presently, the above new schemes are utilized to analyze how the Lagrangian motion of particles is affected by the oscillation angular frequency  $\omega$ . Hence, a range of initial  $\omega$  values is considered and  $\omega$  is modeled as an unknown random parameter. The classic analytical

deterministic flow [68], then becomes stochastic (Figure 5b):

$$\mathbf{v}(t, \mathbf{x}; \omega) = (-\partial_y \phi, \partial_x \phi) \quad \text{with } \phi(\mathbf{x}, t; \omega) = A \sin[\pi f(x, t; \omega)] \sin(\pi y),$$

where  $f(x, t; \omega) = \epsilon \sin(\omega t)x^2 + (1 - 2\epsilon \sin(\omega t))x$ ,  $\mathbf{x} = (x, y)$ , and  $\omega$  initially random. The fixed parameter values are here  $A = 0.1$  and  $\epsilon = 0.1$ . The goal is to provide solutions to the SPDE (6), up to time  $t = 10$  and for  $\omega$  uniformly distributed within  $[\pi/10, 8\pi/10]$ .

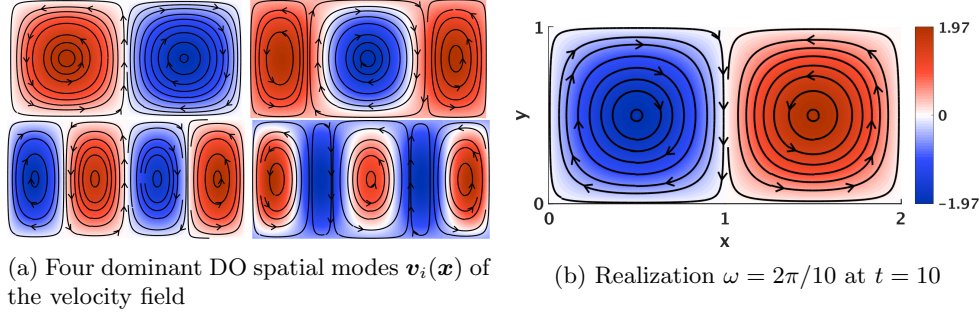


Fig. 5: Stochastic double gyre flow with an initially random oscillation angular frequency. Streamlines are overlaid on the colored intensity of the vorticity.

For the DO computations, the spatial domain  $[0, 2] \times [0, 1]$  is discretized using a  $257 \times 129$  grid with  $l_{bc} = 2 \times 768$  boundary nodes, and the stochastic domain  $[\pi/10, 8\pi/10]$  with  $m = 10,000$  realizations  $\omega_\alpha$  uniformly distributed according to

$$\omega_\alpha = \frac{\pi}{10} + \left( \frac{\alpha - 1}{m - 1} \right) \frac{7\pi}{10}, \quad 1 \leq \alpha \leq m.$$

Hence, in this example,  $l = 2 \times (257 \times 129 - 768) = 64,770$ . The threshold used for increasing the stochastic dimensionality (eq. (46)) is set to  $\sigma = 10^{-2}$ . The retraction used in the DO time-marching is that of section 3.3.3, computed with the gradient descent of Algorithm 1b.

The stochastic velocity is decomposed onto 4 time-independent modes  $\mathbf{v}_i(\mathbf{x})$  (Figure 5), and coefficients  $\beta_i(t; \omega) = \langle \mathbf{v}_i(\mathbf{x}), \mathbf{v}(t, \mathbf{x}; \omega) \rangle$  are obtained by orthogonal projection. They force the SPDE (6). The initial value  $\psi(0, \mathbf{x}; \omega) = \mathbf{x}$  of the flow-map solution is shown on Figure 6.

To first validate the fully linear 6th-order-central-RK3-Shapiro-filter scheme selected in subsection 3.1, the PDE (6) is first solved directly backward in time (forward flowmap) for a fixed value of  $\omega = 2\pi/10$  until  $t = 10$ , and contrasted with the popular 5th order WENO scheme combined with the TVDRK3 time stepping [54]. The two solutions and their differences are shown on Figure 7. As it is expected from the 1D example (Figure 3), the fully linear scheme induces very small numerical errors near shocks, either by smearing or overshooting small details. Indeed, the two flow-map solutions obtained are very comparable, which demonstrates the broad applicability of this fully linear scheme for advection (e.g., they are used in ocean modeling [34, 23, 22]). It is therefore employed next to solve the DO equations (21) as discussed in section 3.

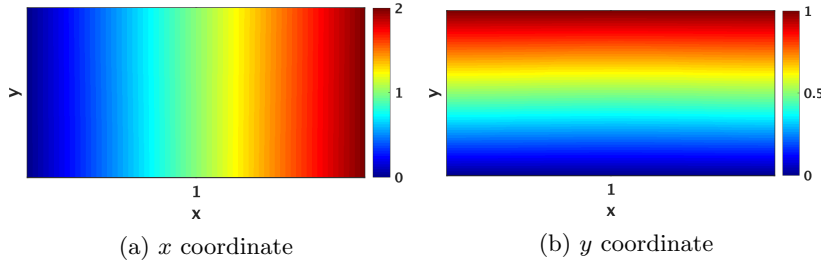


Fig. 6: Initial value  $\psi(0, \mathbf{x}; \omega) = \mathbf{x}$  of the advection eq. (6)

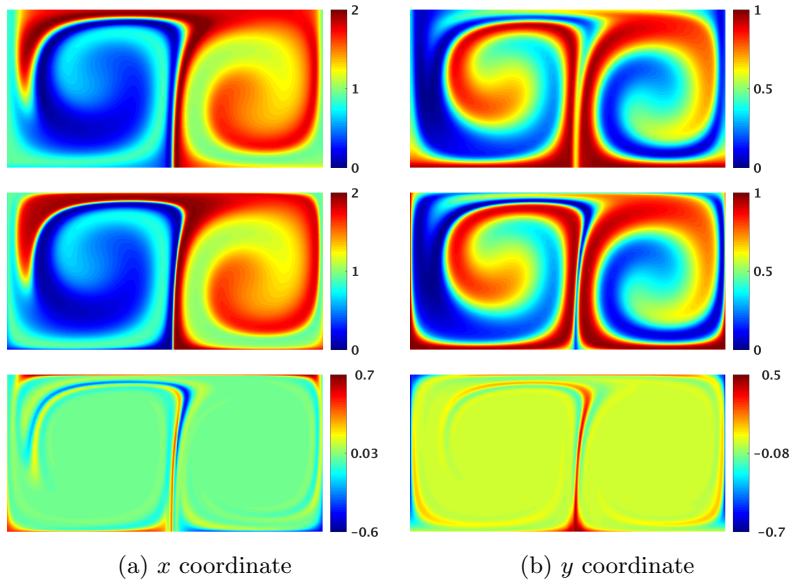


Fig. 7: Comparison between linear 6th-order-central-RK3-Shapiro-filter (*top*) and non linear WENO-TVDRK3 (*middle*) advection schemes for the deterministic solutions of (6) run backward in time (without model order reduction), for the realization  $\omega = 2\pi/10$ , the difference being plotted below (*bottom*).

The stochastic (forward) flow-map DO simulation (21) is run with  $r_\Psi = 20$  modes. For numerical stability, the 8th order Shapiro filter  $\mathcal{F}^{(8)}$  (eq. (30)) is applied at every time step instead of every 10 as in Figure 7. The first 4 DO modes obtained from the truncated SVD at  $t = 10$  are displayed on Figure 8. This figure illustrates the ability of the DO solution to capture dominant modes that are spatially localized and that include shocks (hence far from being Fourier modes), and multi-modal distributions of the coefficients that are far from being Gaussian.

Three deterministic flow-map realizations, obtained by solving directly the transport PDE (6) for  $\omega \in \{2\pi/10, 5\pi/10, 8\pi/10\}$ , are compared to the corresponding DO solutions on Figure 9. The figure shows an excellent agreement which is a key result. The approximation of the solution by 20 modes incurs the loss of some sharp features,

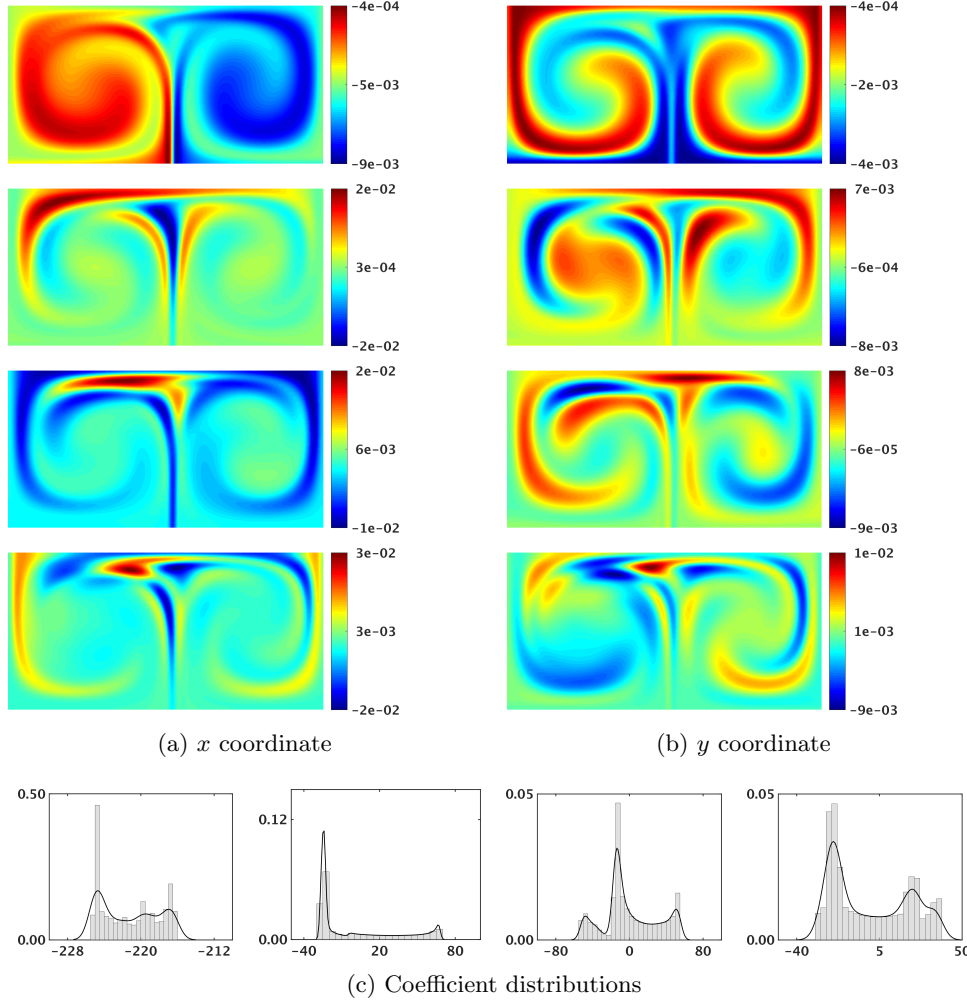


Fig. 8: Dominant four first SVD modes  $\psi_i$  (from top to bottom) and histogram of the corresponding distributions of the coefficients  $\zeta_i$  (from left to right) of the forward flow-map DO solution  $\psi$  for the Double Gyre example at  $t = 10$ .

but the agreement between Monte-Carlo and DO realizations shows that the stochasticity of the flow-map is well captured by the low dimensional time-dependent DO basis. The CPU time (with Matlab) required by the DO simulation for  $m = 10,000$  realizations is  $\text{CPU}_{\text{DO}} = 3,530$ . That of each Monte-Carlo realization requires  $\text{CPU}_{\text{MC}} = 135$ . The observed computational speed-up is therefore  $\frac{\text{CPU}_{\text{MC}} \times m}{\text{CPU}_{\text{DO}}} \simeq 382$ . This is consistent with the prediction given by the ratio  $\frac{lm}{(l+m)r_\psi - r_\psi^2} \simeq 433$  between the dimension of the ambient space and that of the manifold  $\mathcal{M}$ .

The mean and the standard deviation fields of the stochastic flow-map are computed efficiently in a straightforward manner from the DO decomposition and displayed on Figure 10. These results highlight the mean behavior of the flow-map (Panels a and b) and the regions characterized by an increased level of uncertainty



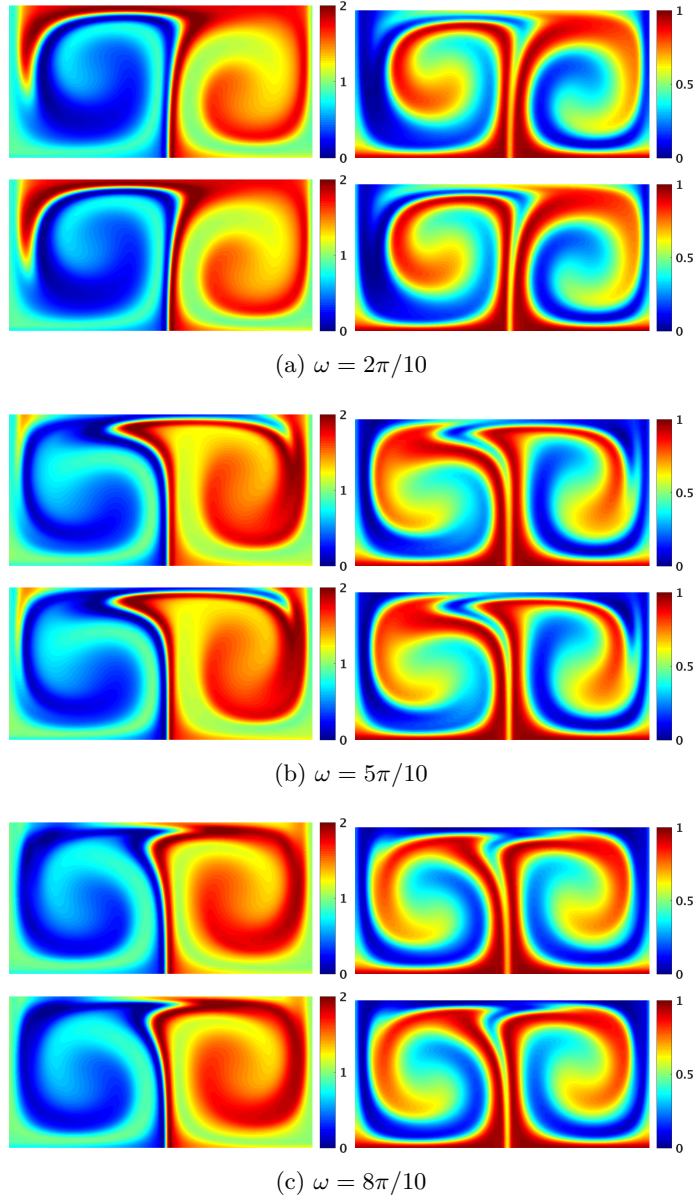
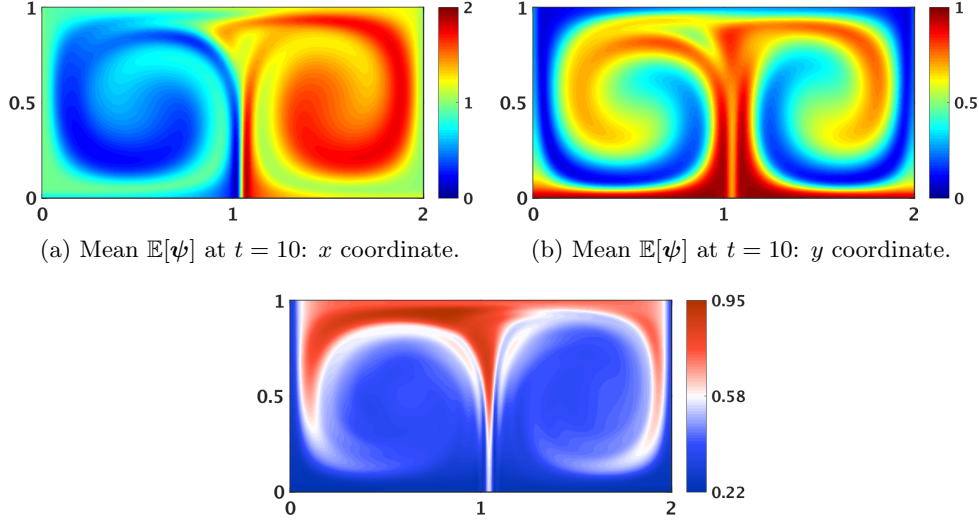


Fig. 9: Evaluation of the DO results (*above*) by comparison with direct MC simulations (*below*) for three double-gyre frequencies  $\omega$  and for both  $x$  (*left column*) and  $y$  (*right column*) coordinates for the forward flow-map. The color scale is identical to that of Figure 6.

(Panel c). They confirm that neither the mean fields nor the standard deviation field are symmetric with respect to the  $y$ -axis at  $t = 10$  because  $\omega$  is uniformly distributed within  $[\pi/10, 8\pi/10]$ . At that time, positions with the largest flow-map uncertainties are located at low  $y$ -values, near the two extreme  $x$ -values. These results critically illustrate the applicability of the new DO schemes for the study of Lagrangian trans-



ports under a stochastic velocity field.



(c) Standard deviation field  $\sigma_\Psi = \mathbb{E}[\|\Psi - \mathbb{E}[\Psi]\|^2]^{1/2}$  for the stochastic flow-map of the double gyre flow at  $t = 10$ . Red highlights initial positions characterized with the most uncertainty.

Fig. 10: Statistical quantities of the stochastic forward flow-map for the double-gyre flow at  $t = 10$ , as computed from the stochastic DO simulation. For (a) and (b), the color scale is identical to that of Figure 6.

**4.2. Stochastic flow past a cylinder.** The stochastic flow past a cylinder is now considered, as a more realistic uncertain flow field. The non-dimensional flow is set on a domain of size 16-by-6 and discretized on a  $240 \times 90$  grid with  $l_{bc} = 2 \times 176$  boundary or obstacle nodes. The Reynolds number is  $\text{Re}=100$ . The cylinder is a disc of center  $(x_c, y_c) = (4.5, 3)$  and of radius  $R = 0.5$ . The flow enters at the left side on the domain with a velocity  $\mathbf{v} = (1, 0)$ . Neumann boundary conditions are considered at the top and bottom walls, while the second normal derivative is set to  $\partial^2 \mathbf{v} / \partial n^2 = 0$  at the outlet on the right. A random perturbation is used to initiate a stochastic flow  $\mathbf{v}(t, \mathbf{x}; \omega)$  with periodic regime.

For the DO flow-map computations (6),  $m = 10,000$  realizations of the flow are obtained from a DO simulation of the Navier Stokes equations with the numerical schemes described in [81]. The time window considered is  $[0, 10]$  and the initial time  $t = 0$  is started once the periodic regime is established. Hence, in this example,  $l = 2(240 \times 90 - 176) = 42,848$ . The threshold for increasing the stochastic dimensionality (eq. (46)) is again set to  $\sigma = 10^{-2}$  and the retraction is that of section 3.3.3 computed with Algorithm 1b.

The stochastic DO velocity initialization is illustrated on Figure 11. The first four dominant modes of this flow along with one particular realization are shown. The stochastic (forward) flow-map is computed analogously to the previous example with  $r_\Psi = 20$  modes and the Shapiro filter  $\mathcal{F}^{(8)}$  being applied at every time step. Figure 12 displays the values of the first 4 dominant modes and the corresponding coefficient distributions of the SVD (eq. (22)) of the flow-map solution at time  $t = 10$ .

Three particular deterministic forward flow-map realizations  $\omega_1$ ,  $\omega_2$ , and  $\omega_3$  are

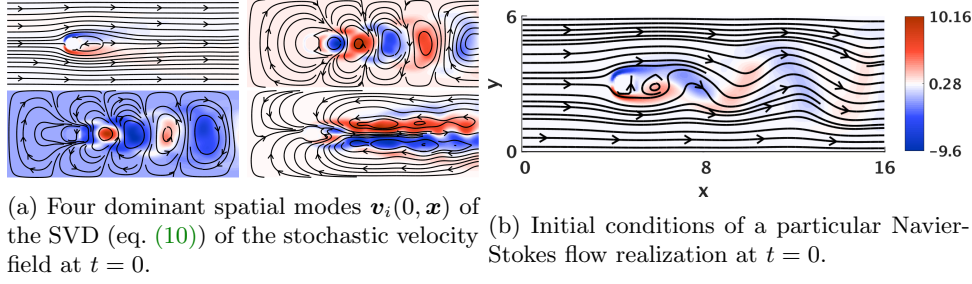


Fig. 11: Stochastic flow past of a cylinder: stochastic DO velocity initialization. Streamlines are overlaid on the colored intensity of the vorticity.

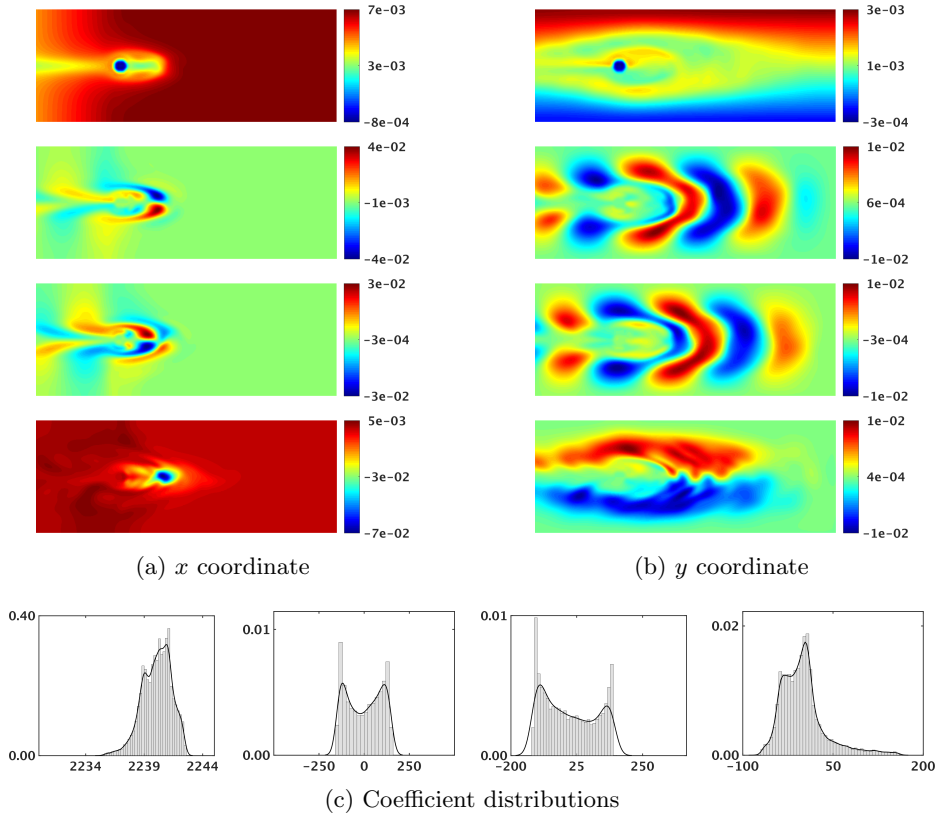


Fig. 12: Dominant four first SVD (eq. (22)) modes  $\psi_i$  and histogram of the corresponding distributions of the coefficients  $\zeta_i$  of the forward flow-map DO solution  $\psi$  for the Flow Past a Cylinder example at  $t = 10$ .

evaluated directly and compared to the corresponding DO solution on Figure 13. Again, an excellent agreement is observed between the MC realizations and the DO reconstructed solutions.

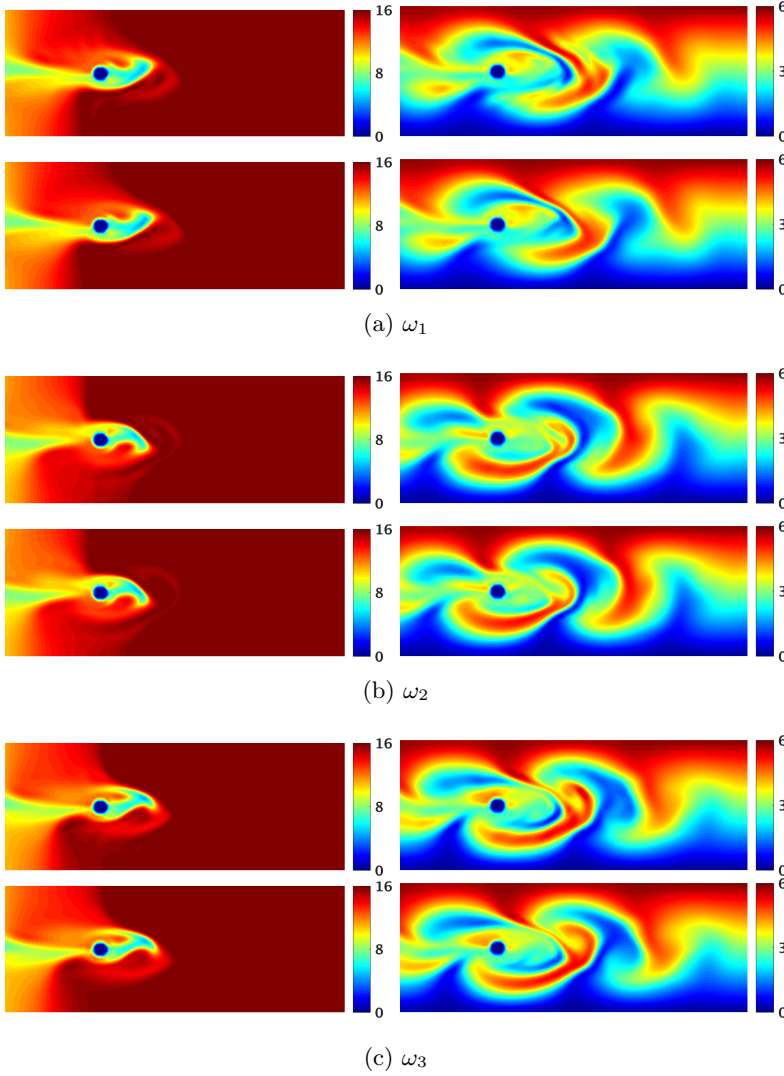


Fig. 13: Evaluation of the DO results (*above*) by comparison with direct MC simulations (*below*) for three forward flow-map realizations for  $\omega_1$ ,  $\omega_2$ ,  $\omega_3$  and for both  $x$  (*left column*) and  $y$  (*right column*) coordinates. The color scale is identical to that of Figure 6.

Similarly as above, the mean and standard deviation fields of the resulting Lagrangian motion are shown on Figure 14. Since particles may exit the domain, the value of  $\psi(10, \mathbf{x}; \omega)$  is the final position occupied by a particle initially located at  $\mathbf{x}$  at time  $t = 0$  if this particle does not leave the domain, or the position of where the particle left the domain otherwise. Recall that here  $l = 42,848$  and  $m = 10,000$ . The observed CPU times required for the forward flow-map DO simulation and one Monte-Carlo realization are respectively  $\text{CPU}_{\text{DO}} = 940$  and  $\text{CPU}_{\text{MC}} \simeq 32$ . This yields an effective computational speed-up of  $\frac{\text{CPU}_{\text{MC}} \times m}{\text{CPU}_{\text{DO}}} \simeq 340$ , still consistent with the prediction  $\frac{lm}{(l+m)r_{\Psi} - r_{\Psi}^2} \simeq 405$ .

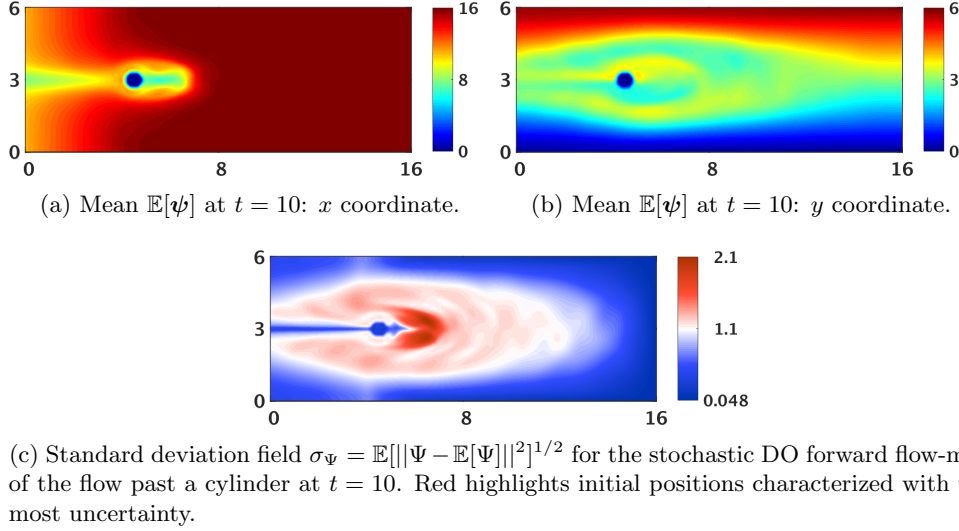


Fig. 14: Statistical quantities of the stochastic DO forward flow-map corresponding to the stochastic flow past a cylinder at  $t = 10$ , itself computed from a stochastic DO Navier-Stokes simulation. For (a) and (b), the color scale is identical to that of Figure 6.

**5. Conclusion.** The Dynamically Orthogonal (DO) decomposition and its geometric interpretations were utilized to obtain systematic optimal reduced-order discrete equations and novel numerical schemes for stochastic advection and Lagrangian transport. The implementation of the DO methodology was thoroughly reviewed and improved by exploiting its relation to the dynamically truncated Singular Value Decomposition. Its broad applicability to treat advection was illustrated, offering a novel efficient method for computing a large number of realizations of the flow-map of an ODE with stochastic velocity. Fully linear, high-order stabilized advection schemes were shown to provide deterministic-stochastic consistency and compatible reduced-order schemes for dynamic linear model order reduction. A set of schemes were provided and utilized to account for the curvature of the fixed rank manifold, to dynamically evolve the rank of the reduced solution, and to ensure the smooth evolution of the orthonormal modes. The effectiveness of the novel time-marching DO equations and numerical schemes for uncertain Lagrangian transport was demonstrated on the analytic stochastic double gyre flow, a benchmark for Lagrangian Coherent Structures studies, and on stochastic velocity data obtained from a numerical simulation of the flow past a cylinder, a sensitive test for advection schemes.

**Acknowledgments.** We thank the MSEAS group at MIT for insightful discussions. We are grateful to the Office of Naval Research for support under grants N00014-14-1-0725 (Bays-DA) and N00014-14-1-0476 (Science of Autonomy – LEARNs) and to the National Science Foundation for support under grant EAR-1520825 (Hazards SEES – ALPHA), each to the Massachusetts Institute of Technology.

## REFERENCES

- [1] P.-A. ABSIL AND J. MALICK, *Projection-like retractions on matrix manifolds*, SIAM Journal on Optimization, 22 (2012), pp. 135–158.
- [2] L. AMBROSIO, *Transport equation and cauchy problem for non-smooth vector fields*, in Calculus of variations and nonlinear partial differential equations, Springer, 2008, pp. 1–41.
- [3] A. BENNETT, *Lagrangian fluid dynamics*, Cambridge University Press, 2006.
- [4] F. BOYER, *Trace theorems and spatial continuity properties for the solutions of the transport equation*, Differential and integral equations, 18 (2005), pp. 891–934.
- [5] R. W. BROCKETT, *Dynamical systems that sort lists, diagonalize matrices and solve linear programming problems*, in Decision and Control, 1988., Proceedings of the 27<sup>th</sup> IEEE Conference on, IEEE, IEEE, 1988, pp. 799–803.
- [6] G.-H. COTTET AND P. D. KOUMOUTSAKOS, *Vortex methods: theory and practice*, Cambridge university press, 2000.
- [7] D. N. DAESCU AND I. M. NAVON, *Efficiency of a pod-based reduced second-order adjoint model in 4d-var data assimilation*, International Journal for Numerical Methods in Fluids, 53 (2007), pp. 985–1004.
- [8] J. DEHAENE, *Continuous-time matrix algorithms systolic algorithms and adaptive neural networks*, PhD thesis, 1995.
- [9] R. J. DiPERNA AND P.-L. LIONS, *Ordinary differential equations, transport theory and sobolev spaces*, Inventiones mathematicae, 98 (1989), pp. 511–547.
- [10] A. DOOSTAN, R. G. GHANEM, AND J. RED-HORSE, *Stochastic model reduction for chaos representations*, Computer Methods in Applied Mechanics and Eng., 196 (2007), pp. 3951–3966.
- [11] D. R. DURRAN, *The third-order adams-bashforth method: An attractive alternative to leapfrog time differencing*, Monthly weather review, 119 (1991), pp. 702–720.
- [12] A. EDELMAN, T. A. ARIAS, AND S. T. SMITH, *The Geometry of Algorithms with Orthogonality Constraints*, SIAM Journal on Matrix Analysis and Applications, 20 (1998), pp. 303–353.
- [13] M. A. EL-BELTAGY, M. I. Wafa, AND O. H. GALAL, *Upwind finite-volume solution of stochastic burgers’ equation*, AM, 03 (2012), pp. 1818–1825.
- [14] B. ENGQUIST, P. LÖTSTEDT, AND B. SJÖGREEN, *Nonlinear filters for efficient shock computation*, Mathematics of Computation, 52 (1989), pp. 509–537.
- [15] R. ERRICO, *What is an adjoint model?*, Bull. Am. Meteorol. Soc., 78 (1997), p. 2577.
- [16] B. FARRELL AND P. IOANNOU, *Generalized stability theory part I: autonomous operators*, J. Atmos. Sci., 53 (1996), pp. 2025–2040.
- [17] F. FEPPON AND P. F. J. LERMUSIAUX, *A geometric approach to dynamical model order reduction*, Submitted to SIAM Journal on Matrix Analysis and Applications, (2017).
- [18] S. K. GODUNOV, *A difference method for numerical calculation of discontinuous solutions of the equations of hydrodynamics*, Matematicheskii Sbornik, 89 (1959), pp. 271–306.
- [19] V. M. GOLOVIZNIN, V. N. SEMENOV, I. A. KOROTKIN, AND S. A. KARABASOV, *A novel computational method for modelling stochastic advection in heterogeneous media*, Transport in porous media, 66 (2007), pp. 439–456.
- [20] A. GRIFFA, A. KIRWAN JR, A. J. MARIANO, T. ÖZGÖKMEN, AND H. T. ROSSBY, *Lagrangian analysis and prediction of coastal and ocean dynamics*, Cambridge University Press, 2007.
- [21] A. GUPTA AND P. F. J. LERMUSIAUX, *Boundary conditions for stochastic DO equations*, MSEAS Report, Dep. of Mechanical Engineering, MIT, Cambridge, MA, 2016.
- [22] P. J. HALEY, JR., A. AGARWAL, AND P. F. J. LERMUSIAUX, *Optimizing velocities and transports for complex coastal regions and archipelagos*, Ocean Modeling, 89 (2015), pp. 1–28.
- [23] P. J. HALEY, JR. AND P. F. J. LERMUSIAUX, *Multiscale two-way embedding schemes for free-surface primitive equations in the “Multidisciplinary Simulation, Estimation and Assimilation System”*, Ocean Dynamics, 60 (2010), pp. 1497–1537.
- [24] P. J. HALEY, JR. AND P. F. J. LERMUSIAUX, *Limiters for Shapiro filtering with primitive-equation ocean models*, MSEAS Report, Department of Mechanical Engineering, Massachusetts Institute of Technology, Cambridge, MA, 2016.
- [25] G. HALLER, *Lagrangian coherent structures*, Annual Review of Fluid Mechanics, 47 (2015), pp. 137–162.
- [26] P. HOLMES, J. L. LUMLEY, AND G. BERKOOZ, *Turbulence, coherent structures, dynamical systems and symmetry*, Cambridge university press, 1998.
- [27] R. A. HORN AND C. R. JOHNSON, *Matrix Analysis*, Cambridge University Press (CUP), 2009.
- [28] M. JARDAK, C.-H. SU, AND G. E. KARNIADAKIS, *Spectral polynomial chaos solutions of the stochastic advection equation*, Journal of Scientific Computing, 17 (2002), pp. 319–338.
- [29] E. KALNAY, *Atmospheric modeling, Data assimilation and Predictability*, Cam. U. Press, 2002.
- [30] O. KOCH AND C. LUBICH, *Dynamical low-rank approximation*, SIAM Journal of Matrix analysis

- and applications, 29 (2007), pp. 434–454.
- [31] J. N. KUTZ, S. L. BRUNTON, B. W. BRUNTON, AND J. L. PROCTOR, *Dynamic mode decomposition: Data-driven modeling of complex systems*, 2016.
  - [32] F. LAFON AND S. OSHER, *High order filtering methods for approximating hyperbolic systems of conservation laws*, Journal of Computational Physics, 96 (1991), pp. 110–142.
  - [33] F. LEKIEN, C. COULLIETTE, A. J. MARIANO, E. H. RYAN, L. K. SHAY, G. HALLER, AND J. MARSDEN, *Pollution release tied to invariant manifolds: A case study for the coast of florida*, Physica D: Nonlinear Phenomena, 210 (2005), pp. 1–20.
  - [34] P. F. LERMUSIAUX, *Error subspace data assimilation methods for ocean field estimation: theory, validation and applications*, Harvard University, 1997.
  - [35] P. F. J. LERMUSIAUX, *Data assimilation via Error Subspace Statistical Estimation, part II: Mid-Atlantic Bight shelfbreak front simulations, and ESSE validation*, Monthly Weather Review, 127 (1999), pp. 1408–1432.
  - [36] P. F. J. LERMUSIAUX, *Estimation and study of mesoscale variability in the Strait of Sicily*, Dynamics of Atmospheres and Oceans, 29 (1999), pp. 255–303.
  - [37] P. F. J. LERMUSIAUX, *Evolving the subspace of the three-dimensional multiscale ocean variability: Massachusetts bay*, Journal of Marine Systems, 29 (2001), pp. 385–422.
  - [38] P. F. J. LERMUSIAUX, *On the mapping of multivariate geophysical fields: Sensitivities to size, scales, and dynamics*, J. of Atmospheric and Oceanic Technology, 19 (2002), pp. 1602–1637.
  - [39] P. F. J. LERMUSIAUX, *Uncertainty estimation and prediction for interdisciplinary ocean dynamics*, Journal of Computational Physics, 217 (2006), pp. 176–199.
  - [40] P. F. J. LERMUSIAUX, D. G. M. ANDERSON, AND C. J. LOZANO, *On the mapping of multivariate geophysical fields: Error and variability subspace estimates*, Quarterly Journal of the Royal Meteorological Society, 126 (2000), pp. 1387–1429.
  - [41] P. F. J. LERMUSIAUX, C.-S. CHIU, G. G. GAWARKIEWICZ, P. ABBOT, A. R. ROBINSON, R. N. MILLER, P. J. HALEY, JR, W. G. LESLIE, S. J. MAJUMDAR, A. PANG, AND F. LEKIEN, *Quantifying uncertainties in ocean predictions*, Oceanography, 19 (2006), pp. 92–105.
  - [42] P. F. J. LERMUSIAUX AND F. LEKIEN, *Dynamics and Lagrangian coherent structures in the ocean and their uncertainty*, in Dynamical System Methods in Fluid Dynamics Oberwolfach Workshop, J. E. Marsden and J. Scheurle, eds., Germany, Jul. 31st - Aug. 6th 2005, Mathematisches Forschungsinstitut Oberwolfach, p. 2.
  - [43] P. F. J. LERMUSIAUX AND A. R. ROBINSON, *Data assimilation via Error Subspace Statistical Estimation, part I: Theory and schemes*, Monthly Wea. Rev., 127 (1999), pp. 1385–1407.
  - [44] S. LEUNG, *An Eulerian approach for computing the finite time Lyapunov exponent*, Journal of computational physics, 230 (2011), pp. 3500–3524.
  - [45] S. LEUNG, *The backward phase flow method for the eulerian finite time lyapunov exponent computations*, Chaos: An Interdisciplinary Journal of Nonlinear Science, 23 (2013), p. 043132.
  - [46] M. LEUTBECHER AND T. PALMER, *Ensemble forecasting*, Journal of Computational Physics, 227 (2008), pp. 3515 – 3539. Predicting weather, climate and extreme events.
  - [47] R. J. LEVEQUE, *Finite volume methods for hyperbolic problems*, vol. 31, Cam. U. Press, 2002.
  - [48] T. LOLLA, *Path planning in time dependent flows using level set methods*, master's thesis, Department of Mechanical Engineering, Massachusetts Institute of Technology, Sep. 2012.
  - [49] C. LUBICH AND I. V. OSELEDETS, *A projector-splitting integrator for dynamical low-rank approximation*, BIT Numerical Mathematics, 54 (2014), pp. 171–188.
  - [50] B. MISHRA, G. MEYER, S. BONNABEL, AND R. SEPULCHRE, *Fixed-rank matrix factorizations and riemannian low-rank optimization*, Computational Statistics, 29 (2014), pp. 591–621.
  - [51] A. MOORE AND R. KLEEMAN, *The singular vectors of a coupled ocean-atmosphere model of ENSO. I: Thermodynamics, energetics and error growth*, Quarterly Journal of the Royal Meteorological Society, 123 (2007), p. 953.
  - [52] E. MUSHARBASH, F. NOBILE, AND T. ZHOU, *Error Analysis of the Dynamically Orthogonal Approximation of Time Dependent Random PDEs*, SIAM Journal on Scientific Computing, 37 (2015), pp. A776–A810.
  - [53] R. ONKEN, A. R. ROBINSON, P. F. J. LERMUSIAUX, P. J. HALEY, AND L. A. ANDERSON, *Data-driven simulations of synoptic circulation and transports in the Tunisia-Sardinia-Sicily region*, Journal of Geophysical Research: Oceans, 108 (2003).
  - [54] S. OSHER AND R. FEDKIW, *Level set methods and dynamic implicit surfaces*, vol. 153, Springer Science & Business Media, 2006.
  - [55] S. OSHER AND C.-W. SHU, *High-order essentially nonoscillatory schemes for hamilton-jacobi equations*, SIAM Journal on numerical analysis, 28 (1991), pp. 907–922.
  - [56] H. OSNES AND H. P. LANGTANGEN, *A study of some finite difference schemes for a unidirectional stochastic transport equation*, SIAM J. on Scientific Comp., 19 (1998), pp. 799–812.
  - [57] T. N. PALMER, J. GELARO, J. BARKMEIJER, AND R. BUIZZA, *Singular vectors, metrics, and*

- adaptive observations*, J. Atmos. Sci., 55 (1998), p. 633.
- [58] A. PAPOULIS AND S. U. PILLAI, *Probability, random variables, and stochastic processes*, McGraw-Hill, (1985).
  - [59] J. QIU AND C.-W. SHU, *On the construction, comparison, and local characteristic decomposition for high-order central WENO schemes*, J. of Comp. Phys., 183 (2002), pp. 187–209.
  - [60] C. W. ROWLEY, *Model reduction for fluids, using balanced proper orthogonal decomposition*, International Journal of Bifurcation and Chaos, 15 (2005), pp. 997–1013.
  - [61] C. W. ROWLEY, I. MEZIĆ, S. BAGHERI, P. SCHLATTER, AND D. S. HENNINGSON, *Spectral analysis of nonlinear flows*, Journal of fluid mechanics, 641 (2009), pp. 115–127.
  - [62] R. M. SAMELSON AND S. WIGGINS, *Lagrangian transport in geophysical jets and waves: The dynamical systems approach*, vol. 31, Springer Science & Business Media, 2006.
  - [63] T. P. SAPSIS AND P. F. J. LERMUSIAUX, *Dynamically orthogonal field equations for continuous stochastic dynamical systems*, Physica D: Nonlinear Phenomena, 238 (2009), pp. 2347–2360. doi:10.1016/j.physd.2009.09.017.
  - [64] T. P. SAPSIS AND P. F. J. LERMUSIAUX, *Dynamically orthogonal field equations for continuous stochastic dynamical systems*, Physica D, 238 (2009), pp. 2347–2360.
  - [65] T. P. SAPSIS AND P. F. J. LERMUSIAUX, *Dynamical criteria for the evolution of the stochastic dimensionality in flows with uncertainty*, Physica D: Nonlinear Phenomena, 241 (2012), pp. 60–76.
  - [66] T. P. SAPSIS, M. P. UECKERMAN, AND P. F. J. LERMUSIAUX, *Global analysis of Navier–Stokes and Boussinesq stochastic flows using dynamical orthogonality*, Journal of Fluid Mechanics, 734 (2013), pp. 83–113.
  - [67] P. J. SCHMID, *Dynamic mode decomposition of numerical and experimental data*, Journal of fluid mechanics, 656 (2010), pp. 5–28.
  - [68] S. C. SHADDEN, F. LEKIEN, AND J. E. MARSDEN, *Definition and properties of lagrangian coherent structures from finite-time lyapunov exponents in two-dimensional aperiodic flows*, Physica D: Nonlinear Phenomena, 212 (2005), pp. 271–304.
  - [69] R. SHAPIRO, *Smoothing, filtering, and boundary effects*, Rev. Geophys., 8 (1970), p. 359.
  - [70] R. SHAPIRO, *The use of linear filtering as a parameterization of atmospheric diffusion*, Journal of the Atmospheric Sciences, 28 (1971), pp. 523–531.
  - [71] R. SHAPIRO, *Linear filtering*, Mathematics of Computation, 29 (1975), pp. 1094–1094.
  - [72] C.-W. SHU AND S. OSHER, *Efficient implementation of essentially non-oscillatory shock-capturing schemes*, Journal of Computational Physics, 77 (1988), pp. 439–471.
  - [73] B. SJÖGREEN, *High order centered difference methods for the compressible navier-stokes equations*, Journal of Computational Physics, 117 (1995), pp. 67–78.
  - [74] S. SMITH, *Dynamical systems that perform the singular value decomposition*, Systems & Control Letters, 16 (1991), pp. 319–327.
  - [75] D. SUBRAMANI AND P. F. J. LERMUSIAUX, *Energy-optimal path planning by stochastic dynamically orthogonal level-set optimization*, Ocean Modeling, (2016). In press.
  - [76] D. TANG, F. W. SCHWARTZ, AND L. SMITH, *Stochastic modeling of mass transport in a random velocity field*, Water Resources Research, 18 (1982), pp. 231–244.
  - [77] L. N. TREFETHEN AND D. BAU III, *Numerical linear algebra*, vol. 50, Siam, 1997.
  - [78] J. TRYÖEN, O. L. MAÏTRE, M. NDJINGA, AND A. ERN, *Intrusive Galerkin methods with upwind-ing for uncertain nonlinear hyperbolic systems*, J. Comp. Phys., 229 (2010), pp. 6485–6511.
  - [79] J. H. TU, C. W. ROWLEY, D. M. LUCHTENBURG, S. L. BRUNTON, AND J. N. KUTZ, *On dynamic mode decomposition: Theory and applications*, J. of Comp. Dyn., 1 (2014), pp. 391–421.
  - [80] M. P. UECKERMAN, P. F. J. LERMUSIAUX, AND T. P. SAPSIS, *Numerical Schemes and Studies for Dynamically Orthogonal Equations of Stochastic Fluid and Ocean Flows*, MSEAS Report 11, Dep. of Mechanical Engineering, MIT, Cambridge, MA, 2011.
  - [81] M. P. UECKERMAN, P. F. J. LERMUSIAUX, AND T. P. SAPSIS, *Numerical schemes for dynamically orthogonal equations of stochastic fluid and ocean flows*, Journal of Computational Physics, 233 (2013), pp. 272–294.
  - [82] X. WAN, D. XIU, AND G. E. KARNIADAKIS, *Stochastic solutions for the two-dimensional advection-diffusion equation*, SIAM J. on Scientific computing, 26 (2004), pp. 578–590.
  - [83] WIKIMEDIA COMMONS, <https://commons.wikimedia.org/wiki/File:tangentialvektor.svg>.
  - [84] M. O. WILLIAMS, I. G. KEVREKIDIS, AND C. W. ROWLEY, *A data-driven approximation of the koopman operator: Extending dynamic mode decomposition*, Journal of Nonlinear Science, 25 (2015), pp. 1307–1346.
  - [85] P. D. WILLIAMS, *Achieving seventh-order amplitude accuracy in leapfrog integrations*, Monthly Weather Review, 141 (2013), pp. 3037–3051.
  - [86] D. XIU AND G. E. KARNIADAKIS, *Modeling uncertainty in flow simulations via generalized polynomial chaos*, Journal of computational physics, 187 (2003), pp. 137–167.